Arousal-induced cortical activity triggers lactate release from astrocytes

Zuend, Marc ; Saab, Aiman S ; Wyss, Matthias T ; Ferrari, Kim David ; Hösli, Ladina ; Looser, Zoe J ; Stobart, Jillian L ; Duran, Jordi ; Guinovart, Joan J ; Barros, L Felipe ; Weber, Bruno

Abstract: It has been suggested that, in states of arousal, release of noradrenaline and -adrenergic signalling affect long-term memory formation by stimulating astrocytic lactate production from glycogen. However, the temporal relationship between cortical activity and cellular lactate fluctuations upon changes in arousal remains to be fully established. Also, the role of -adrenergic signalling and brain glycogen metabolism on neural lactate dynamics in vivo is still unknown. Here, we show that an arousal-induced increase in cortical activity triggers lactate release into the extracellular space, and this correlates with a fast and prominent lactate dip in astrocytes. The immediate drop in astrocytic lactate concentration and the parallel increase in extracellular lactate levels underline an activity-dependent lactate release from astrocytes. Moreover, when -adrenergic signalling is blocked or the brain is depleted of glycogen, the arousal-evoked cellular lactate surges are significantly reduced. We provide in vivo evidence that cortical activation upon arousal triggers lactate release from astrocytes, a rise in intracellular lactate levels mediated by -adrenergic signalling and the mobilization of lactate from glycogen stores.

DOI: https://doi.org/10.1038/s42255-020-0170-4

Arousal-induced cortical activity triggers lactate release from astrocytes

Marc Zuend[1,2], Aiman S Saab[1,2,4], Matthias T Wyss[1,2,4], Kim David Ferrari[1,2], Jillian Stobart[1,2], L Felipe Barros[3] and Bruno Weber[1,2 *]

(1) Institute of Pharmacology and Toxicology, University of Zurich, 8057 Zurich, Switzerland

(2) Neuroscience Center Zurich, University of Zurich and ETH Zurich, 8057 Zurich, Switzerland

(3) Centro de Estudios Científicos, Valdivia 5110466, Chile

(4) These authors contributed equally to this work.

* Correspondence: bweber@pharma.uzh.ch

Abstract

Arousal-induced release of noradrenaline and β-adrenergic signaling impacts long-term memory formation by stimulating astrocytic lactate production. However, the temporal relationship between cortical activity, β-adrenergic signaling and lactate dynamics *in vivo* are poorly understood. Here, we investigated arousal-evoked lactate dynamics in cortical neurons and astrocytes in awake mice. A brief exposure to isoflurane provoked a strong arousal response, pupil dilation and calcium elevations in neurons and astrocytes. Arousal-induced cortical activity triggered an extracellular lactate surge that correlated with a fast and prominent lactate dip in astrocytes. After these initial events we observed a delayed rise in both astrocytic and neuronal lactate. The immediate drop in astrocytic lactate concentration and the subsequent lactate increase in the extracellular space suggests an activity-dependent lactate release from astrocytes. Of interest, is that when β-adrenergic signaling was pharmacologically blocked the evoked lactate rise in both astrocytes and neurons was significantly reduced. We provide here *in vivo* evidence that arousal triggers lactate release from astrocytes and a rise in lactate levels, which is mediated by β-adrenergic signaling.

Introduction

The brain is almost exclusively fueled by glucose oxidation [1,2]. Acute elevations in brain activity are met with a transient net increase in aerobic glycolysis and the production of lactate [3,4] that is released into the extracellular space [5,6]. However, the primary cellular source of this activity-driven lactate release remains a matter of debate [7-11]. A long-standing hypothesis is that astrocytes increase their glycolysis in response to neuronal activity to cover neuronal ATP demand with lactate [8,12]. Many studies have expanded this metabolic support model [3,13-15]. Nevertheless, direct *in vivo* evidence of activity-evoked lactate release from astrocytes to neurons is still unavailable. Clearly, neurons are able to maintain their activity *in vivo* with a lactate supply [16] and an *in vivo* lactate gradient from astrocytes to neurons favors astrocytic shuttling of lactate to neurons [17]. However, recent studies suggest that neurons increase their glycolytic activity upon stimulation and may also release lactate [18].

At a behavioral level, lactate mobilization from glycogen, primarily stored in astrocytes, has been shown to promote long-term memory formation [6,19-22]. In particular, emotionally-driven memory formation induced by stress or arousal, involves β-adrenergic signaling and lactate release from astrocytes [23]. During arousal, noradrenaline released from locus coeruleus projections strongly activates astrocytes [24,25] and could have diverse metabolic functions, including glycogenolysis [26-28]. Apart from serving as an energy substrate, lactate also regulates neuronal excitability by modulating ATP-sensitive potassium (K_{ATP}) channels [29,30] or by direct action on membrane receptors [31,32]. Thus, lactate signaling likely has diverse functions including the regulation of wakefulness, brain plasticity and memory consolidation [8,33].

In this paper, we have addressed the way in which fast changes in cortical activity modulate lactate dynamics in astrocytes and neurons in awake behaving mice. We found that arousal triggers a rapid lactate release from astrocytes, which is followed by increased lactate levels in neurons. Theses arousal-evoked lactate surges were in part mediated by β-adrenergic signaling.

Results

Cortical lactate dynamics in neurons and astrocytes in response to acute isoflurane exposure

We have studied how state-dependent changes in cortical activity impact neuronal and astrocytic lactate levels by using genetically-encoded sensors for lactate, Laconic [34] and calcium, RCaMP 1.07 [35] and GCaMP6s [36] combined with two-photon microscopy imaging in awake behaving mice. (**Figures 1D, E**). Mice were trained for head-restrained, awake two-photon imaging using a suppression-response task with a water reward (**Figures 1A, B**; see Methods for details). Only mice that reached a 75 % correct trial performance during training were included for awake imaging **(Figure 1C)**. During imaging sessions mice were exposed to isoflurane for 20 minutes (1.5 %; **Figure S1A**) while monitoring lactate level changes in cortical neurons and astrocytes (**Figures S1B**, **C**). Volatile anesthetics like isoflurane are well-known to induce changes in cortical activity [37-39]. Exposure to isoflurane caused a significant increase in intracellular lactate levels in both astrocytes and neurons, levels which remained elevated during the isoflurane period (relative lactate signal rose by 4.6 ± 1.6% in neurons and 5.5 ± 2.0 % in astrocytes). Critically, at the onset of isoflurane exposure (within 10-20 s) we observed a significant and transient drop in lactate levels in astrocytes (**Figure S1C**; relative lactate signal dropped by -1.8 ± 1.1 %, $p = 0.03$, Tukey post-hoc test). In contrast, neurons showed no significant lactate decrease when compared to baseline ($p = 0.38$, Tukey post-hoc test; **Figure S1B**). After stopping isoflurane, lactate levels completely recovered to baseline levels within 20.2 ± 6.0 min and 17.7 ± 7.1 min, in neurons and astrocytes respectively. In a similar manner, animal responsiveness and task performance (water licking) recovered within 20.7 ± 9.1 min (data not shown).

Isoflurane exposure causes an initial arousal response before induction of anesthesia

The biphasic lactate response observed in astrocytes upon isoflurane exposure, consisting of an initial dip, followed by a rise in lactate concentration (**Figure S1C**), could be triggered by distinct phases of isoflurane-induced brain states [38]. Isoflurane and other general anesthetics are known to cause an initial arousal before the anesthetized state [39,40]. Hence, we have carefully investigated the way in

which our isoflurane protocol impacts overall brain activity (**Figure S2**) and cortical calcium dynamics in neurons and astrocytes (**Figure S3**).

First, we studied brain activity patterns with electroencephalography (EEG) recordings (**Figures S2A-D**). Indeed, acute exposure to isoflurane did cause changes in EEG patterns (**Figures S2A, B**). Within seconds of isoflurane exposure, we observed a significant increase in high-frequency spectrum typically associated with cortical desynchronization [41,42]. Cortical desynchronization was followed by an increase in slow-wave oscillations until EEG patterns reached the burst suppression found during deep anesthesia [43,44]. The initial EEG band shifts observed upon isoflurane exposure (**Figures S2C, D**) strongly correlated with changes observed during an arousal response [41,45]. This was further corroborated with electromyography (EMG) recordings (**Figure S2E**) as well as measurements of pupil size (**Figure S2F** [39,45,46]). Consistent with our EEG recordings, seconds after isoflurane exposure, EMG electrical activity was significantly increased by 67.6 ± 21.5% and pupil diameter was increased by 51.3 ± 31.7 % (**Figures S2G, H**). In the subsequent anesthetized state, muscle activity (EMG) and pupil size were strongly reduced by 40.1 ± 16.5 % and 47.0 ± 17.1 %, respectively (**Figures S2G**, **H**). Taken together, our EEG, EMG and pupil size measurements identify a rapid and transient arousal response before the onset of the anesthetized state (**Figure S2I**).

Arousal has been shown to evoke cortical calcium bursts in astrocytes [24,25] and neurons [45]. We decided therefore to examine whether isoflurane-induced arousal would similarly lead to a cortical calcium response (**Figure S3**). Using a combination of two genetically-encoded calcium sensors RCaMP1.07 [35] and GCaMP6s [36] expressed in neurons and astrocytes, we monitored cellular calcium dynamics 100-200 µm below the cortical surface with two-photon imaging (**Figures S3B, C**). Immediately upon isoflurane exposure there was a significant calcium elevation in both neurons and astrocytes (in neurons, whole frame fluorescence intensity increased by 24.2 ± 7.3%; $p = 0.015$; **Figure S3B** and in astrocytes, it increased by 84.7 ± 73.6 %; $p < 0.001$; **Figure S3C**). In addition, automated analysis of calcium signals [47,48] revealed a two-fold increase in calcium events in both neurons and astrocytes

(**Figures S3D**, **E**). Noteworthy, was that during the subsequent anesthetized state, whole frame fluorescence intensities for RCaMP1.07 and GCaMP6s were greatly reduced in neurons and astrocytes (-21.0 ± 7.2% and -29.4 ± 4.7%, **Figures S3B, C**). This was also consistent with a substantial loss in spontaneous activity in neurons and astrocytes when compared to baseline activity in the awake state (**Figures S3D, E**) as shown previously [49]. Both calcium fluorescence intensities and event frequencies returned to baseline values when isoflurane application was stopped (**Figures S3B-E**). We find that the overall calcium dynamics observed in astrocytes and neurons are in line with our EEG, EMG and pupillometry measurements.

Arousal triggers lactate release from astrocytes

Our EEG, EMG and pupil size measurements, as well as our cortical calcium recordings, provide convincing evidence that when administered, isoflurane causes an immediate, strong arousal response. Thus, we wondered whether brief isoflurane pulses would lead to arousal-evoked cortical lactate fluctuations. We therefore adapted our protocol and exposed awake mice to a brief 20 s isoflurane pulse (ISO pulse; **Figure 2A**). As expected, the ISO pulse triggered a large pupil dilation without causing subsequent pupil constriction, indicating that we were only seeing an arousal response (**Figure 2B**). This was further corroborated by measuring neuronal and astrocytic calcium dynamics (**Figures 2C**, **D**). The application of an ISO pulse elicited a significant calcium transient in both neurons and astrocytes. Neuronal calcium levels were increased by 18.1 ± 7.2 % (**Figure 2C**) and astrocytic calcium levels by 67.5 ± 34.0 % (**Figure 2D**). Relevant to note, is that we did not observe the pronounced decrease in calcium fluorescence levels that occurred upon prolonged isoflurane exposure. Thus, the ISO pulse would seem to be an effective paradigm for which to study arousal-mediated cortical metabolite dynamics in awake mice.

Next, we examined the way in which arousal impacts lactate levels in cortical neurons and astrocytes. In both neurons and astrocytes, lactate levels were significantly increased by 2.4 ± 1.3 % (**Figure 2E**) and 3.6 ± 1.4 % (**Figure 2F**) respectively. Striking to note was that only in astrocytes revealed a

prominent lactate dip by 2.1 ± 1.4 % before the subsequent lactate surge (**Figure 2F**). This is in line with our earlier observations. We then compared the time courses of the arousal-evoked calcium and lactate responses in neurons and astrocytes (**Figures 2G**, **H**). Arousal-induced calcium and lactate recordings were each performed in the same animal using a multi-viral injection approach (**Figure 1D**; see Methods for details). In neurons, the evoked lactate surge appeared after the calcium transients (**Figure 2G**). In contrast, astrocytic changes in calcium and lactate levels occurred almost simultaneously (**Figure 2H**). The minimum of the astrocytic lactate dip coincided with the peak of the astrocytic calcium response (lactate dip: 0.26 ± 0.14 min vs. calcium peak: 0.18 ± 0.08 min; $p = 0.24$, **Figure 2H**). To further compare response kinetics between neurons and astrocytes, we computed the response slopes (**Figure 2I**) of the lactate elevations. Notably, despite the initial lactate dip, astrocytes displayed a significantly faster lactate rise compared to neurons (lactate slope astrocytes: 8.3 ± 1.1 %/min and lactate slope neurons: 4.7 ± 3.3 %/min; $p < 0.001$, **Figures 2G-I**).

The immediate arousal-mediated decrease in astrocytic lactate suggests an activity-dependent lactate consumption or release. If it were the latter, we might expect to detect an arousal-evoked lactate release from astrocytes with a concomitant increase in extracellular lactate levels. We therefore measured changes in extracellular space (ECS) lactate levels using a pre-calibrated lactate biosensor inserted into the somatosensory cortex (**Figure 3A**; see Methods for details). A brief isoflurane pulse caused extracellular lactate to rise significantly by 1.10 ± 0.15 mM (**Figures 3B, C**). Two distinct slopes were seen in these elevated ECS lactate levels. There was an initial, rapid lactate rise (S1: 25.8 ± 6.3 µM/s) that peaked around 35 s post stimulus, which was followed by a second, significantly slower component (S2: 8.1 ± 3.8 µM/s; **Figures 3B, C**). We went on to compare the kinetics of the ECS, astrocytes, and neurons (**Figures 3D-F**). Two distinct phases in lactate dynamics were identifiable during the first 60 seconds: (I) A fast initial ECS lactate rise that coincided with the lactate decrease in astrocytes and (II) a slow delayed ECS lactate rise that coincided with the neuronal lactate increase (**Figure 3F**). The significant differences in lactate dynamics between the three compartments were further corroborated by direct comparison of the time series of lactate level changes and kinetics

within the initial 60 s of the arousal response (**Figures 3G-I**). Our data implies that arousal leads to rapid lactate release from astrocytes.

β-adrenergic signaling mediates arousal-induced lactate level surges

Noradrenaline, released form locus coeruleus projections during arousal events, has a strong impact on cortical activity [46,50] and is involved in modulating numerous cellular processes [24,25,51]. In astrocytes, β-adrenergic signaling has been reported to shape emotionally-driven memory formation [23] and it is suggested that lactate shuttling from astrocytes to neurons plays a key role [6,19,22]. Our experiments show that arousal impacts cortical lactate dynamics and that astrocytes are likely to release lactate upon cortical activation **(Figures 2, 3)**. Our next test was to see whether β-adrenergic signaling mediates arousal-induced lactate dynamics.

We used propranolol (10 mg/kg, i.p.), a non-selective β-adrenergic receptor blocker [27,52], to study how β-adrenergic signaling affects arousal-evoked calcium and lactate responses in astrocytes and neurons (**Figures 4** and **S5**). Calcium and lactate recordings were performed before (0 h) and at several timepoints (1, 3, 6 and 24 h) after administering propranolol (**Figure 4A**). With accurate, repetitive imaging, we followed arousal-evoked responses in the same cells over time (**Figure S4**). Blocking β-adrenergic receptors with propranolol did not impair evoked calcium transients in either neurons or astrocytes **(Figure S5**), a finding in line with previous reports [24,25]. In contrast, propranolol had a significant impact on the induced lactate surges in both astrocytes and neurons (**Figures 4B, C, E, F**), but caused no overt changes in the astrocytic lactate dip (**Figure 4D**). Lactate surges (**Figure 4E**) and response slopes (**Figure 4F**) started to decrease compared to baseline responses within the first hour after drug injection. Six hours after propranolol injection, arousal-evoked lactate surges, measured as the area under curve (AUC), were reduced by 49.4 ± 40.2 % and 31.2 ± 32.5 % ($p < 0.001$ and $p < 0.001$). We also saw that the response slopes decreased by 35.3 ± 28.6 % and 34.7 ± 25.3 % ($p < 0.001$ and $p = 0.004$) compared to baseline responses in neurons and astrocytes, respectively. Twenty-four hours after injection of propranolol, lactate responses recovered completely. Control experiments with

186 saline injections did not show any changes in the arousal-evoked calcium and lactate responses (**Figure**
187 **S6**). In summary, β-adrenergic signaling appears to primarily regulate lactate production and
188 mobilization rather than acting directly on the astrocytic lactate release machinery **(Figure 5)**.

Discussion

Acute brain activation is accompanied by an increase in aerobic glycolysis and surges in extracellular lactate [5,6]. Our work here shows that arousal in mice elicits transient lactate elevations in cortical astrocytes, neurons and the extracellular space **(Figure 3)**. Analysis of the temporal lactate dynamics in the three brain compartments revealed that astrocytes rapidly release lactate upon activation, with a corresponding rise in extracellular lactate. Neuronal lactate levels increased after the initial astrocytic lactate release concomitant with a slowing of the extracellular lactate surge. Our results thus provide evidence for arousal-induced astrocyte-to-neuron lactate shuttling in awake mice.

New arousal paradigm during awake imaging in mice

We have introduced here a new paradigm to elicit a robust and reproducible non-motor evoked arousal response in awake mice, with two-photon microscopy used for high spatiotemporal imaging. Acute exposure to isoflurane induces a rapid arousal response [38,39], which we identified carefully by measuring EEG, EMG, pupil size and cortical calcium responses. Pupil dilation occurred within seconds of an isoflurane stimulus. Tracking pupil diameter changes is a consistent method for monitoring wakefulness, switching between cortical states and arousal [39,45,46]. Our EEG recordings during the initial seconds of isoflurane exposure are also in line with EEG profiles obtained from cortical responses to locus coeruleus stimulation [50,53]. The activity of locus coeruleus projections is critical in the regulation of wakefulness and in promoting arousal [54,55]. Arousal induced by forced locomotion or by air puffs has been shown to evoke calcium transients in cortical astrocytes [24,25,56] and in neurons [45]. In a similar manner, our isoflurane-induced arousal protocol triggered a robust calcium response in both astrocytes and neurons. Important to note, is that by limiting isoflurane exposure to a brief 20 s pulse, we only produce arousal, while avoiding the subsequent sedative state that appears after prolonged isoflurane administration **(Figure 2)**. This is substantiated by EEG, EMG, pupillometry and cellular calcium measurements that clearly allow for differentiation between the arousal response and the anaesthetized state **(Figure S2)**. Moreover, a short 20 s isoflurane pulse avoids possible isoflurane side effects, such as the partial mitochondrial depolarization reported in cardiomyocytes after 15-30 min

of isoflurane application [57,58]. We successfully established the isoflurane pulse paradigm to reliably evoke arousal in the absence of locomotion [46]. Isoflurane is also a very strong sensory stimulus [38,39] and can be easily combined with behavioral training (water licking performance) during awake two-photon imaging **(Figures 1, 2)**.

Arousal triggers lactate release from astrocytes

We used genetically-encoded sensors for calcium [35,36] and lactate [34] expression in cortical astrocytes and neurons to examine intracellular calcium and lactate dynamics in response to isoflurane-induced arousal **(Figure 2)**. Moreover, with a pre-calibrated Pinnacle lactate biosensor [17,59,60] inserted into the cortex, we also studied arousal-evoked lactate fluctuations in the ECS (**Figure 3)**. While monitoring lactate dynamics with high temporal resolution, we detected a rapid and significant lactate level decrease in only astrocytes upon arousal. The astrocytic lactate dip occurred almost simultaneously with the arousal-evoked calcium transients (**Figure 2**). In principle, this dip in astrocytic lactate could either be due to an increase in lactate consumption (conversion to pyruvate) or to an increased release of lactate. If the latter, then we would expect a corresponding, rapid increase in ECS lactate levels. Indeed, arousal-evoked ECS lactate dynamics revealed two distinct lactate response slopes. Striking to see was an initial, fast increase in ECS lactate of about 26 µM/s that coincided with the astrocytic lactate dip, suggesting that the rapid extracellular lactate rise is promoted by lactate release from astrocytes (**Figure 3**). A very similar fast lactate release from astrocytes has been reported in response to acute extracellular [K^+] elevations *in vitro*, to electrical stimulation *in vivo* and in hippocampal slices [13,61]. Hence, a rise in extracellular [K^+] during neuronal activity could rapidly stimulate neighboring astrocytes to release lactate, either through a lactate channel [13], monocarboxylate transporters [62] or possibly via pannexins [63].

Arousal strongly induced cortical circuit activation as revealed by EEG and neuronal calcium recordings (**Figures S2 and S3**), in line with other studies [24,25,38,45]. Neuronal stimulation was recently suggested to trigger neuronal lactate release [18]. However, arousal-induced neuronal activation did not have a

neuronal lactate dip that corresponded with an extracellular lactate rise. On the contrary, neurons mainly showed increased lactate levels after the initial astrocytic lactate release **(Figures 2, 3).** This finding was not unexpected as it has been previously shown that neurons have a fast activity-dependent calcium response but a delayed glycolytic response [18]. In fact, the neuronal lactate increase coincides with a significant slowing of the extracellular lactate rise (3-fold decrease), suggesting that the neuronal lactate rise is driven by lactate uptake (**Figure 3**). Although neuronal activity may also stimulate glycolysis in neurons [18], it seems unlikely that neurons contain sufficient lactate for it to be released instantaneously. Astrocytes, on the other hand, have a higher basal glycolytic activity [64] as well as higher intracellular lactate levels *in vivo* [17]. Thus, lactate release from this "pressure reservoir" in astrocytes could be rapidly triggered for export in an activity-dependent manner [65].

The arousal-evoked lactate dip in astrocytes is directly followed by a lactate overshoot. This is best explained by having lactate production (aerobic glycolysis) surpassing lactate release. The extracellular lactate elevation period parallels the astrocytic and neuronal lactate surges, suggesting that an increased lactate production is strongly linked to lactate release and uptake respectively **(Figure 5)**. Many activity-dependent neuronal signals have been shown to trigger lactate production by glycogenolysis and glycolysis in astrocytes. Astrocytic glycolysis has been seen to be promoted by glutamate, ammonium, nitric oxide and K^+ [12-14,66] and glycogen breakdown is stimulated by vasoactive intestinal peptide, adenosine, noradrenaline and K^+ [28,67]. However, in response to arousal, the primary signal responsible for the astrocytic lactate production may well be noradrenaline as we discuss below.

β-adrenergic signaling and arousal-induced lactate mobilization from astrocytes

During arousal, noradrenaline is released throughout the brain from locus coeruleus projections [68]. Noradrenergic signaling has been implicated in cognition and memory formation [69-71], particularly involving β-adrenergic receptors [72-74]. A recent study highlighted that β_2-adrenergic signaling in astrocytes is critical for emotionally-driven memory consolidation in mice [23]. Blocking β-adrenergic signaling either pharmacologically with propranolol or by shRNA-mediated knockdown in astrocytes

but not in neurons, impaired long-term memory formation, which could be rescued by administering extracellular lactate [23]. This impairment was attributed to noradrenaline-mediated glycogen breakdown and lactate release [28], which was reported to be important for long-term memory formation [6,19]. Astrocytic β-adrenergic signaling may also impact glucose metabolism [27,75,76].

We hypothesized that if β-adrenergic signaling is required to mobilize lactate in astrocytes, then we should see a perturbation of arousal-evoked cortical lactate dynamics with pharmacological inhibition. Indeed, 1 to 6 hours after a single intraperitoneal injection of propranolol (10 mg/kg), lactate surges in both astrocytes and neurons were strongly reduced (**Figure 4**). Notably, the astrocytic lactate dip was not overtly perturbed indicating that β-adrenergic signaling may not be necessary to facilitate lactate channel opening and/or transporter activity. In fact, astrocytes and neurons remained responsive to arousal-induced cortical activation, as calcium transients were not diminished by blocking β-adrenergic receptors (**Figure S5**). This is in line with arousal-mediated astrocytic calcium transients being primarily mediated by α-adrenergic but not β-adrenergic receptors [24,25]. Hence, other activity-dependent mechanisms could stimulate the lactate release machinery in astrocytes, very likely mediated by an acute extracellular [K^+] rise [13,61]. High [K^+] may also participate in the delayed increase in astrocytic lactate, through NBCe1-mediated stimulation of glycolysis [61,77,78] and glycogen degradation [67], acting in concert with the slower stimulation of astrocytic glycolysis by glutamate [12,77].

Important to note is that while both astrocytes and neurons remained similarly responsive to arousal, indicating that workload and energy demand were unchanged during propranolol treatment, the subsequent reductions in arousal-evoked lactate surges in neurons and astrocytes are primarily caused by a partial deficit in lactate production. In astrocytes, but not in neurons, β-adrenergic signaling has been shown to impact emotionally-driven memory consolidation through a lactate-mediated mechanism [23]. Thus, we assume that reductions in arousal-evoked lactate elevations in neurons are directly linked to a reduced lactate mobilization presumably from glycogen stores in astrocytes **(Figures 4, 5)**. Although direct effects of β-adrenergic signaling on lactate production in cortical

297 neurons cannot be ruled out, it is more likely that astrocytes are critically involved in arousal-evoked
298 lactate mobilization, since glycogen is predominantly stored in astrocytes [79,80], and lactate derived from
299 glycogenolysis promotes memory formation [19] with a common lactate-dependent mechanism that is
300 mediated by β-adrenergic signaling in astrocytes [23].
301
302 Inhibition of β-adrenergic signaling via a single intraperitoneal propranolol injection (10 mg/kg)
303 reduced arousal-evoked lactate surges in astrocytes by about 35 % around 6 h post injection (**Figure 4**).
304 It could well be that β-adrenergic receptors were not fully inhibited by a single intraperitoneal injection
305 and that a higher or prolonged dose, or a locally administered dose may even have an even stronger
306 impact on glycogen or glucose metabolism, as previously suggested [23,81]. As discussed above, other
307 activity-dependent mechanisms are also likely to be involved in promoting lactate production, such as
308 K^+-mediated acceleration of glycolysis and glycogenolysis [67,77]. Nonetheless, it is most interesting that
309 a minimal perturbation of β-adrenergic signaling has such a strong impact on cortical lactate dynamics.
310
311 In summary, our data favors an activity-induced astrocyte-to-neuron lactate shuttle. We provide *in*
312 *vivo* evidence to show that arousal triggers lactate release from astrocytes and that astrocytic lactate
313 mobilization is partly mediated by β-adrenergic signaling **(Figure 5)**. This opens an exciting avenue for
314 future studies to dissect activity-dependent mechanisms involved in lactate release and the dynamic
315 interplay between astrocytes and neurons in the awake animal. Recent studies increasingly highlight
316 that lactate is more than just an energy substrate and is critically involved in diverse signaling
317 mechanisms [8,29-33]. Hence, arousal-mediated lactate release from astrocytes could be crucial in fine-
318 tuning neuronal network activity and brain plasticity, which may also have clinical implications for
319 various psychiatric disorders.
320

Methods

Animals

All experimental and surgical procedures were approved by the local veterinary authorities according to the guidelines of the Swiss Animal Protection Law, Veterinary Office, Canton Zurich (Act of Animal Protection, 16 December 2005 and Animal Protection Ordinance, 23 April 2008). Female C57BL/6J (Charles River) mice weighing between 20 and 30 g were used in this study. All mice were kept in standardized single cages with food and water *ad libitum*. During experimental periods mice were subjected to water deprivation. Body weight was monitored before and after all training and experimental sessions. If body weight loss exceeded 15 % with respect to the baseline weight animals would be given free access to water until their weight had normalized. All housed animals were subjected to a 12/12 h light/dark cycle with the dark phase adjusted so that the animals were in their active phase during experimental periods. Surgical interventions were performed at age 10-15 weeks.

Surgical interventions

Surgical interventions were performed on two separate days. On the first day, the animals were anesthetized with isoflurane 1.5-2.0 % in a mixture of O_2 and air (30/70 %) at a flow rate of 400 ml/min. Vitamin A ointment was applied to avoid corneal desiccation. To prevent dehydration 0.2 ml of saline solution was subcutaneously injected every hour. Animals were fixed in a stereotaxic frame (Model 900; David Kopf Instruments) for the head-post implantation as previously described by Mayrhofer, et al. [82]. In short, fur from the head and neck area was removed and after disinfection (Kodan; Schülke & Mayr) a 2 cm long midline incision was made between the eyes to the neck. A bonding agent (Gluma Comfort; Heraeus Kulzer) was applied after cleaning the skull and carefully separating the temporal muscle. Next, a head-cap was formed, made of multiple layers of light-curing dental cement (Synergy D6 Flow, Coltene AG). Finally, a custom-made aluminum head-post was attached, and open skin was attached to the implant with acrylic glue (Histoacryl; Braun).

On the second day, a craniotomy was performed using a dental drill (OSSEODOC; Bien-Air), above the left somatosensory cortex, for intracortical virus injection. Animals were anesthetized with a mixture

of fentanyl (0.05 mg/kg bodyweight; Sintenyl, Sintetica), midazolam (5 mg/kg bodyweight; Dormicum, Roche), and medetomidine (0.5 mg/kg bodyweight; Domitor, Orion Pharma) injected intraperitoneally, and anesthesia was maintained with midazolam after 50 min (5 mg/kg bodyweight, subcutaneous). A facemask delivering oxygen was installed to prevent hypoxemia.

For multi-viral injections in the somatosensory cortex, neighboring adeno-associated viral (AAV) injections (50-75 nl each) were delivered with a custom-made micro injector as described elsewhere [17] to achieve multiple non-overlapping loci in the somatosensory cortex. The neuronal construct included a human synapsin-1 (hSYN) promoter and the astrocyte-specific construct included a minimal GFAP promoter (gfaABC$_1$D). Transfection was performed by injecting: (A) a lactate sensor *Laconic* for neuronal (San Martin, et al. [34]; AAV6-hSYN-Laconic; titer 1.02 E13 VG/ml); (B) for astrocytic (AAV9-GFAP-Laconic; titer 3.1 E12 VG/ml); (C) calcium sensors RCaMP 1.07 for neuronal [35]; AAV6-hSYN-RCaMP 1.07; titer 2.4 E13 VG/ml) and (D) GCaMP6s for astrocytic (Chen, et al. [36]; AAV9-GFAP-GCaMP6s; titer 3.2 E13 VG/ml) expression, diluted 5-30 times in physiological saline. Injections were performed via a glass capillary to a cortical depth of 300 µm through the intact dura. Large blood vessels were avoided to prevent bleeding and the absorption of light by hemoglobin during imaging. For later chronic optical measurements, a square sapphire glass (3×3 mm, Powatec GmbH) was gently placed on the dura mater and sealed with light-curing dental cement (Synergy D6 Flow, Coltene AG).

Behavioral training

A custom-made head fixation box was built for chronic imaging and constant positioning of the animal. The response-suppression task used in this study was designed to suppress movement for 8 s periods while images from the cortex were acquired. After 8 s a tone was sounded to indicate the end of each period (reward stimulus). As a reward stimulus a 70 dB click noise of 1 ms duration with 2-18 kHz bandwidth was produced (background noise was 50 dB) and delivered by stereo speakers positioned 20 cm away from the animals' head. A drinking spout that included a piezo sensor (LDT0-028K; Measurement Specialties) was mounted in front of the animal. The spout was connected to a solenoid valve (Type 0330; Burkert) that controlled water delivery upon spout deflection. A custom-made piezo

movement sensor for monitoring movement was positioned under the animals' body. A camera (191133; Conrad Electronic AG) with an infrared light source (BL0106-15-28; Kingbright Electronics) was used for monitoring animals. We used the custom-written LabVIEW program (National Instruments) and multifunctional data acquisition cards to control and monitor all components of the behavioral apparatus [83]. We used a similar protocol to that developed by Mayrhofer, et al. [83] to adapt the animals to the experimental environment. Animals were first handled and familiarized with the experimenter, one week after implantation, for at least 3 times a day. They were adapted to water deprivation 12 h before training sessions and accustomed to tolerate head fixation and to drink water from a spout every 2 s during training sessions. Finally, the animals were trained in two daily sessions not to move for up to 8 s until the reward stimulus was presented. Occurrence of movement during this period led to a temporal delay of the reward stimulus. Delay was computed depending on the time point and the duration of movement within the normal movement-suppression window. After sounding of each tone, the animal was given a 1.5-second-long "window of opportunity" to lick on the spout. After the reward stimulus was triggered by a spout deflection (stimulus-response), there was a water release of 0.002 ml water per trial (referred to as "reward on lick"). All licks were registered. Licks within the suppression window were counted as false licks. Detected licks within the window of opportunity were counted as correct trials. We computed the number of correct trials for each training session to evaluate performance and training progress of all animals.

Isoflurane experiments

In the first set of experiments we collected 10 min baseline (50 trials) where the animal was performing the behavioral paradigm, followed by isoflurane administration for 20 min (1.5 % isoflurane in O_2 and air (1:2) and 400 ml/min total flow rate) and a recovery phase after turning isoflurane off, for 30 min without anesthesia. In the second set of experiments a baseline of 5 min was acquired followed by administration of isoflurane for 20 s (1.5 %) and a recovery phase of 14 min and 40 s. This protocol was also used for 5 sequential imaging sessions at 1, 3, 6 and 24 h after the initial recording at 0 h.

EEG, EMG, pupil size and ECS recordings

Electroencephalogram (EEG), electromyogram (EMG) and extracellular glucose and lactate measurements were performed with a commercially-available recording system (4-channel EEG/EMG/BIO Tethered System; Pinnacle Technology). All mice had a head-post mounted as previously described and regions of interest were spared from dental cement. Two to five days after the head-post was mounted, the skull was opened with a dental drill. Two EEG screws were implanted bilaterally in the frontal area, 2 screws (#8403; Pinnacle Technology) in the occipital area, a guide cannula (#7032; Pinnacle Technology) was implanted into the primary somatosensory cortex, wired with a head mount (#8402; Pinnacle Technology) and fixed with dental cement. Two EMG electrodes were placed in the neck muscle of the animal. After a recovery period of 2 weeks, the pre-calibrated lactate biosensor (#7004; Pinnacle Technology) was inserted into the guide cannula. Prior to implantation each lactate biosensor was calibrated *in vitro* to ensure selectivity and sensitivity for lactate. Data was acquired at 250 Hz for EEG and 1 Hz for lactate measurements. For pupil size measurements the camera (see above) for monitoring the animal was used, having the pupil approximated as a circle-like structure with a custom-written MATLAB algorithm used to compute changes in pupil radius.

Microscope design and imaging parameters

A custom-made two-photon laser scanning microscope [84] equipped with a two-photon laser with <120 fs temporal pulse width (InSight DeepSee Dual; Spectra-Physics) with a 20x water immersion objective (W Plan-Apochromat 20x/1.0 DIC VIS-IR; Zeiss) was used for image acquisition. Excitation and emission beam paths were separated by a dichroic mirror (F73-825; AHF Analysentechnik). A dichroic mirror at 506nm (F38-506; AHF Analysentechnik) and 560nm (F38-560; AHF Analysentechnik) separated the emission light beam. The emission light was focused on the photomultiplier (H9305-03, Hamamatsu) by two lenses (LA1050-A1 and AL5040-A2; Thorlabs). We used emission filters for blue (F39-477; AHF Analysentechnik), green and yellow (F37-545; AHF Analysentechnik) and red (F39-608; AHF Analysentechnik) for multi-color imaging. Data was acquired from the somatosensory cortex 100-200

μm below the cortical surface. Anatomical imaging was performed at a resolution of 512×512 pixels at a frequency of 0.74 Hz. Emission signals were acquired at 11.84 Hz and with a 128×256-pixel resolution. ScanImage [85] and custom-written LabVIEW software (National Instruments) were used for image control and data acquisition.

Drug application

Propranolol, a β-adrenergic receptor antagonist, in saline, was injected intraperitoneally (i.p.) at a concentration of 10 mg/kg. For control experiments, only saline was injected.

Data analysis and statistics

Data processing and analysis was carried out with MATLAB 2017a (MathWorks, Natick, USA) and ImageJ [86]. Calcium and ratiometric data was analyzed with the MATLAB toolbox Cellular and Hemodynamic Image Processing Suite [47]. Regions of interest (ROIs) were manually selected in ImageJ using high resolution 512×512-pixel images. All calcium data was analyzed with the activity-based plugin FLIKA in CHIPS. For data cross-correlation corrplot from MATLAB's econometrics toolbox was used, with a Pearson's linear correlation coefficient at a significance level of 0.05. The MATLAB plotter function was used to compute data distribution histogram of correlated data. Statistical analyses were performed with t-test. Experimental means were used for time series comparison. For numerical integrations of the area under the curve (AUC), the MATLAB trapz function was used. Statistical analyses and calculations were performed in R using the lme4 package [87] for linear mixed-effects models and multivariate analysis. All data was reported and plotted as uncorrected means and standard deviation of the means (SD). P values for different parameter comparisons were obtained using the lsmeans or multcomp [88] packages with Tukey post-hoc tests. P values < 0.05 were considered significant and are indicated with an asterisk, P values < 0.01 with two and P values < 0.001 with three asterisks.

Acknowledgements

We thank all lab members of the Weber group for support and frequent discussions. We would also like to thank Jean-Charles Paterna and the Viral Vector Facility of the Neuroscience Center Zurich (ZNZ) for viral productions. We further thank Johannes M. Mayrhofer and Wolfger von der Behrens for their initial support in establishing the suppression-response task. A.S.S. is supported by a Synapsis Career Fellowship Award, M.T.W. is supported by the Hartmann-Müller Foundation, L.F.B. is funded by the Chilean Government through the Centers of Excellence Basal Financing Program of CONICYT, and B.W. is supported by the Swiss National Science Foundation (SNF Number: 31003A_156965) and is a member of the Clinical Research Priority Program Molecular Imaging Network (MINZ).

Author contributions

Conceptualization, M.Z., A.S.S., M.T.W. and B.W.; Methodology, M.Z.; Software, M.Z. and K.D.F.; Formal Analysis, M.Z. and A.S.S.; Investigation, M.Z.; Resources: J.L.S. and L.F.B.; Writing – Original Draft M.Z. and A.S.S.; Visualization: M.Z. and A.S.S.; Writing – Review & Editing, M.Z., A.S.S., M.T.W., L.F.B. and B.W.; Supervision and Project Administration, M.T.W. and B.W.; Funding Acquisition, A.S.S., M.T.W. and B.W.

Declaration of Interests

The authors declare no competing interests.

References

1 Kety, S. S. & Schmidt, C. F. The Nitrous Oxide Method for the Quantitative Determination of Cerebral Blood Flow in Man: Theory, Procedure and Normal Values. *J Clin Invest* **27**, 476-483, doi:10.1172/JCI101994 (1948).

2 Sokoloff, L. Localization of functional activity in the central nervous system by measurement of glucose utilization with radioactive deoxyglucose. *Journal of cerebral blood flow and metabolism : official journal of the International Society of Cerebral Blood Flow and Metabolism* **1**, 7-36, doi:10.1038/jcbfm.1981.4 (1981).

3 Prichard, J. *et al.* Lactate rise detected by 1H NMR in human visual cortex during physiologic stimulation. *Proceedings of the National Academy of Sciences of the United States of America* **88**, 5829-5831 (1991).

4 Fox, P. T., Raichle, M. E., Mintun, M. A. & Dence, C. Nonoxidative glucose consumption during focal physiologic neural activity. *Science* **241**, 462-464 (1988).

5 Hu, Y. & Wilson, G. S. A temporary local energy pool coupled to neuronal activity: fluctuations of extracellular lactate levels in rat brain monitored with rapid-response enzyme-based sensor. *Journal of neurochemistry* **69**, 1484-1490 (1997).

6 Newman, L. A., Korol, D. L. & Gold, P. E. Lactate produced by glycogenolysis in astrocytes regulates memory processing. *PloS one* **6**, e28427, doi:10.1371/journal.pone.0028427 (2011).

7 Yellen, G. Fueling thought: Management of glycolysis and oxidative phosphorylation in neuronal metabolism. *The Journal of cell biology* **217**, 2235-2246, doi:10.1083/jcb.201803152 (2018).

8 Magistretti, P. J. & Allaman, I. Lactate in the brain: from metabolic end-product to signalling molecule. *Nature reviews. Neuroscience* **19**, 235-249, doi:10.1038/nrn.2018.19 (2018).

9 Dienel, G. A. Lack of appropriate stoichiometry: Strong evidence against an energetically important astrocyte-neuron lactate shuttle in brain. *Journal of neuroscience research* **95**, 2103-2125, doi:10.1002/jnr.24015 (2017).

10 Barros, L. F. & Weber, B. CrossTalk proposal: an important astrocyte-to-neuron lactate shuttle couples neuronal activity to glucose utilisation in the brain. *The Journal of physiology* **596**, 347-350, doi:10.1113/JP274944 (2018).

11 Bak, L. K. & Walls, A. B. CrossTalk opposing view: lack of evidence supporting an astrocyte-to-neuron lactate shuttle coupling neuronal activity to glucose utilisation in the brain. *The Journal of physiology* **596**, 351-353, doi:10.1113/JP274945 (2018).

12 Pellerin, L. & Magistretti, P. J. Glutamate uptake into astrocytes stimulates aerobic glycolysis: a mechanism coupling neuronal activity to glucose utilization. *Proceedings of the National Academy of Sciences of the United States of America* **91**, 10625-10629 (1994).

13 Sotelo-Hitschfeld, T. *et al.* Channel-mediated lactate release by K(+)-stimulated astrocytes. *The Journal of neuroscience : the official journal of the Society for Neuroscience* **35**, 4168-4178, doi:10.1523/JNEUROSCI.5036-14.2015 (2015).

14 Lerchundi, R. *et al.* NH4(+) triggers the release of astrocytic lactate via mitochondrial pyruvate shunting. *Proceedings of the National Academy of Sciences of the United States of America* **112**, 11090-11095, doi:10.1073/pnas.1508259112 (2015).

15 Lin, A. L., Fox, P. T., Hardies, J., Duong, T. Q. & Gao, J. H. Nonlinear coupling between cerebral blood flow, oxygen consumption, and ATP production in human visual cortex. *Proceedings of the National Academy of Sciences of the United States of America* **107**, 8446-8451, doi:10.1073/pnas.0909711107 (2010).

16 Wyss, M. T., Jolivet, R., Buck, A., Magistretti, P. J. & Weber, B. In vivo evidence for lactate as a neuronal energy source. *The Journal of neuroscience : the official journal of the Society for Neuroscience* **31**, 7477-7485, doi:10.1523/JNEUROSCI.0415-11.2011 (2011).

17 Machler, P. *et al.* In Vivo Evidence for a Lactate Gradient from Astrocytes to Neurons. *Cell metabolism* **23**, 94-102, doi:10.1016/j.cmet.2015.10.010 (2016).

18 Diaz-Garcia, C. M. *et al.* Neuronal Stimulation Triggers Neuronal Glycolysis and Not Lactate Uptake. *Cell metabolism* **26**, 361-374 e364, doi:10.1016/j.cmet.2017.06.021 (2017).

19 Suzuki, A. *et al.* Astrocyte-neuron lactate transport is required for long-term memory formation. *Cell* **144**, 810-823, doi:10.1016/j.cell.2011.02.018 (2011).

20 Zhang, Y. *et al.* Inhibition of Lactate Transport Erases Drug Memory and Prevents Drug Relapse. *Biological psychiatry* **79**, 928-939, doi:10.1016/j.biopsych.2015.07.007 (2016).

21 Duran, J., Saez, I., Gruart, A., Guinovart, J. J. & Delgado-Garcia, J. M. Impairment in long-term memory formation and learning-dependent synaptic plasticity in mice lacking glycogen synthase in the brain. *Journal of cerebral blood flow and metabolism : official journal of the International Society of Cerebral Blood Flow and Metabolism* **33**, 550-556, doi:10.1038/jcbfm.2012.200 (2013).

22 Gibbs, M. E., Anderson, D. G. & Hertz, L. Inhibition of glycogenolysis in astrocytes interrupts memory consolidation in young chickens. *Glia* **54**, 214-222, doi:10.1002/glia.20377 (2006).

23 Gao, V. *et al.* Astrocytic beta2-adrenergic receptors mediate hippocampal long-term memory consolidation. *Proceedings of the National Academy of Sciences of the United States of America* **113**, 8526-8531, doi:10.1073/pnas.1605063113 (2016).

24 Paukert, M. *et al.* Norepinephrine controls astroglial responsiveness to local circuit activity. *Neuron* **82**, 1263-1270, doi:10.1016/j.neuron.2014.04.038 (2014).

25 Ding, F. *et al.* alpha1-Adrenergic receptors mediate coordinated Ca2+ signaling of cortical astrocytes in awake, behaving mice. *Cell Calcium* **54**, 387-394, doi:10.1016/j.ceca.2013.09.001 (2013).

26 Alberini, C. M., Cruz, E., Descalzi, G., Bessieres, B. & Gao, V. Astrocyte glycogen and lactate: New insights into learning and memory mechanisms. *Glia* **66**, 1244-1262, doi:10.1002/glia.23250 (2018).

27 Dienel, G. A. & Cruz, N. F. Aerobic glycolysis during brain activation: adrenergic regulation and influence of norepinephrine on astrocytic metabolism. *Journal of neurochemistry* **138**, 14-52, doi:10.1111/jnc.13630 (2016).

28 Sorg, O. & Magistretti, P. J. Characterization of the glycogenolysis elicited by vasoactive intestinal peptide, noradrenaline and adenosine in primary cultures of mouse cerebral cortical astrocytes. *Brain research* **563**, 227-233 (1991).

29 Sada, N., Lee, S., Katsu, T., Otsuki, T. & Inoue, T. Epilepsy treatment. Targeting LDH enzymes with a stiripentol analog to treat epilepsy. *Science* **347**, 1362-1367, doi:10.1126/science.aaa1299 (2015).

30 Clasadonte, J., Scemes, E., Wang, Z., Boison, D. & Haydon, P. G. Connexin 43-Mediated Astroglial Metabolic Networks Contribute to the Regulation of the Sleep-Wake Cycle. *Neuron* **95**, 1365-1380 e1365, doi:10.1016/j.neuron.2017.08.022 (2017).

31 Tang, F. *et al.* Lactate-mediated glia-neuronal signalling in the mammalian brain. *Nature communications* **5**, 3284, doi:10.1038/ncomms4284 (2014).

32 Morland, C. *et al.* The lactate receptor, G-protein-coupled receptor 81/hydroxycarboxylic acid receptor 1: Expression and action in brain. *Journal of neuroscience research* **93**, 1045-1055, doi:10.1002/jnr.23593 (2015).

33 Barros, L. F. Metabolic signaling by lactate in the brain. *Trends in neurosciences* **36**, 396-404, doi:10.1016/j.tins.2013.04.002 (2013).

34 San Martin, A. *et al.* A genetically encoded FRET lactate sensor and its use to detect the Warburg effect in single cancer cells. *PloS one* **8**, e57712, doi:10.1371/journal.pone.0057712 (2013).

35 Ohkura, M., Sasaki, T., Kobayashi, C., Ikegaya, Y. & Nakai, J. An improved genetically encoded red fluorescent Ca2+ indicator for detecting optically evoked action potentials. *PloS one* **7**, e39933, doi:10.1371/journal.pone.0039933 (2012).

36 Chen, T. W. *et al.* Ultrasensitive fluorescent proteins for imaging neuronal activity. *Nature* **499**, 295-300, doi:10.1038/nature12354 (2013).

37 Franks, N. P. General anaesthesia: from molecular targets to neuronal pathways of sleep and arousal. *Nature reviews. Neuroscience* **9**, 370-386, doi:10.1038/nrn2372 (2008).

38 Liu, X. *et al.* Arousal transitions in sleep, wakefulness, and anesthesia are characterized by an orderly sequence of cortical events. *NeuroImage* **116**, 222-231, doi:10.1016/j.neuroimage.2015.04.003 (2015).

39 Kum, J. E., Han, H. B. & Choi, J. H. Pupil Size in Relation to Cortical States during Isoflurane Anesthesia. *Exp Neurobiol* **25**, 86-92, doi:10.5607/en.2016.25.2.86 (2016).

40 Guedel, A. E. *Inhalation anesthesia; a fundamental guide*. (Macmillan, 1951).

41 Chen, C. R. *et al.* Roles of adrenergic alpha1 and dopamine D1 and D2 receptors in the mediation of the desynchronization effects of modafinil in a mouse EEG synchronization model. *PloS one* **8**, e76102, doi:10.1371/journal.pone.0076102 (2013).

42 McCormick, D. A. & Bal, T. Sleep and arousal: thalamocortical mechanisms. *Annu Rev Neurosci* **20**, 185-215, doi:10.1146/annurev.neuro.20.1.185 (1997).

43 Jameson, L. C. & Sloan, T. B. Using EEG to monitor anesthesia drug effects during surgery. *J Clin Monit Comput* **20**, 445-472, doi:10.1007/s10877-006-9044-x (2006).

44 MacIver, M. B. & Bland, B. H. Chaos analysis of EEG during isoflurane-induced loss of righting in rats. *Frontiers in systems neuroscience* **8**, 203, doi:10.3389/fnsys.2014.00203 (2014).

45 Reimer, J. *et al.* Pupil fluctuations track fast switching of cortical states during quiet wakefulness. *Neuron* **84**, 355-362, doi:10.1016/j.neuron.2014.09.033 (2014).

46 Vinck, M., Batista-Brito, R., Knoblich, U. & Cardin, J. A. Arousal and locomotion make distinct contributions to cortical activity patterns and visual encoding. *Neuron* **86**, 740-754, doi:10.1016/j.neuron.2015.03.028 (2015).

47 Barrett, M. J. P., Ferrari, K. D., Stobart, J. L., Holub, M. & Weber, B. CHIPS: an Extensible Toolbox for Cellular and Hemodynamic Two-Photon Image Analysis. *Neuroinformatics* **16**, 145-147, doi:10.1007/s12021-017-9344-y (2018).

48 Stobart, J. L. *et al.* Cortical Circuit Activity Evokes Rapid Astrocyte Calcium Signals on a Similar Timescale to Neurons. *Neuron* **98**, 726-735 e724, doi:10.1016/j.neuron.2018.03.050 (2018).

602 49 Thrane, A. S. *et al.* General anesthesia selectively disrupts astrocyte calcium signaling in the
603 awake mouse cortex. *Proceedings of the National Academy of Sciences of the United States of*
604 *America* **109**, 18974-18979, doi:10.1073/pnas.1209448109 (2012).
605 50 Carter, M. E. *et al.* Tuning arousal with optogenetic modulation of locus coeruleus neurons.
606 *Nature neuroscience* **13**, 1526-1533, doi:10.1038/nn.2682 (2010).
607 51 Reimer, J. *et al.* Pupil fluctuations track rapid changes in adrenergic and cholinergic activity in
608 cortex. *Nature communications* **7**, 13289, doi:10.1038/ncomms13289 (2016).
609 52 Baker, J. G. The selectivity of beta-adrenoceptor antagonists at the human beta1, beta2 and
610 beta3 adrenoceptors. *British journal of pharmacology* **144**, 317-322,
611 doi:10.1038/sj.bjp.0706048 (2005).
612 53 Berridge, C. W. & Foote, S. L. Effects of locus coeruleus activation on electroencephalographic
613 activity in neocortex and hippocampus. *The Journal of neuroscience : the official journal of the*
614 *Society for Neuroscience* **11**, 3135-3145 (1991).
615 54 Aston-Jones, G. & Cohen, J. D. An integrative theory of locus coeruleus-norepinephrine
616 function: adaptive gain and optimal performance. *Annu Rev Neurosci* **28**, 403-450,
617 doi:10.1146/annurev.neuro.28.061604.135709 (2005).
618 55 Berridge, C. W. & Waterhouse, B. D. The locus coeruleus-noradrenergic system: modulation of
619 behavioral state and state-dependent cognitive processes. *Brain research. Brain research*
620 *reviews* **42**, 33-84 (2003).
621 56 Srinivasan, R. *et al.* Ca(2+) signaling in astrocytes from Ip3r2(-/-) mice in brain slices and during
622 startle responses in vivo. *Nature neuroscience* **18**, 708-717, doi:10.1038/nn.4001 (2015).
623 57 Ljubkovic, M. *et al.* Isoflurane preconditioning uncouples mitochondria and protects against
624 hypoxia-reoxygenation. *American journal of physiology. Cell physiology* **292**, C1583-1590,
625 doi:10.1152/ajpcell.00221.2006 (2007).
626 58 Sedlic, F. *et al.* Monitoring mitochondrial electron fluxes using NAD(P)H-flavoprotein
627 fluorometry reveals complex action of isoflurane on cardiomyocytes. *Biochimica et biophysica*
628 *acta* **1797**, 1749-1758, doi:10.1016/j.bbabio.2010.07.009 (2010).

59 Dash, M. B., Bellesi, M., Tononi, G. & Cirelli, C. Sleep/wake dependent changes in cortical glucose concentrations. *Journal of neurochemistry* **124**, 79-89, doi:10.1111/jnc.12063 (2013).

60 Naylor, E. *et al.* Lactate as a biomarker for sleep. *Sleep* **35**, 1209-1222, doi:10.5665/sleep.2072 (2012).

61 Ruminot, I., Schmalzle, J., Leyton, B., Barros, L. F. & Deitmer, J. W. Tight coupling of astrocyte energy metabolism to synaptic activity revealed by genetically encoded FRET nanosensors in hippocampal tissue. *Journal of cerebral blood flow and metabolism : official journal of the International Society of Cerebral Blood Flow and Metabolism*, 271678X17737012, doi:10.1177/0271678X17737012 (2017).

62 Pierre, K. & Pellerin, L. Monocarboxylate transporters in the central nervous system: distribution, regulation and function. *Journal of neurochemistry* **94**, 1-14, doi:10.1111/j.1471-4159.2005.03168.x (2005).

63 Karagiannis, A. *et al.* Hemichannel-mediated release of lactate. *Journal of cerebral blood flow and metabolism : official journal of the International Society of Cerebral Blood Flow and Metabolism* **36**, 1202-1211, doi:10.1177/0271678X15611912 (2016).

64 Hung, Y. P., Albeck, J. G., Tantama, M. & Yellen, G. Imaging cytosolic NADH-NAD(+) redox state with a genetically encoded fluorescent biosensor. *Cell metabolism* **14**, 545-554, doi:10.1016/j.cmet.2011.08.012 (2011).

65 Kasparov, S. Are Astrocytes the Pressure-Reservoirs of Lactate in the Brain? *Cell metabolism* **23**, 1-2, doi:10.1016/j.cmet.2015.11.001 (2016).

66 Bolanos, J. P., Delgado-Esteban, M., Herrero-Mendez, A., Fernandez-Fernandez, S. & Almeida, A. Regulation of glycolysis and pentose-phosphate pathway by nitric oxide: impact on neuronal survival. *Biochimica et biophysica acta* **1777**, 789-793, doi:10.1016/j.bbabio.2008.04.011 (2008).

67 Choi, H. B. *et al.* Metabolic communication between astrocytes and neurons via bicarbonate-responsive soluble adenylyl cyclase. *Neuron* **75**, 1094-1104, doi:10.1016/j.neuron.2012.08.032 (2012).

68 Schwarz, L. A. & Luo, L. Organization of the locus coeruleus-norepinephrine system. *Current biology : CB* **25**, R1051-R1056, doi:10.1016/j.cub.2015.09.039 (2015).

69 Sara, S. J., Vankov, A. & Herve, A. Locus coeruleus-evoked responses in behaving rats: a clue to the role of noradrenaline in memory. *Brain Res Bull* **35**, 457-465 (1994).

70 Sara, S. J. The locus coeruleus and noradrenergic modulation of cognition. *Nature reviews. Neuroscience* **10**, 211-223, doi:10.1038/nrn2573 (2009).

71 Gibbs, M. E., Hutchinson, D. S. & Summers, R. J. Noradrenaline release in the locus coeruleus modulates memory formation and consolidation; roles for alpha- and beta-adrenergic receptors. *Neuroscience* **170**, 1209-1222, doi:10.1016/j.neuroscience.2010.07.052 (2010).

72 Cahill, L., Prins, B., Weber, M. & McGaugh, J. L. Beta-adrenergic activation and memory for emotional events. *Nature* **371**, 702-704, doi:10.1038/371702a0 (1994).

73 Murchison, C. F. *et al.* A distinct role for norepinephrine in memory retrieval. *Cell* **117**, 131-143 (2004).

74 Sun, H., Mao, Y., Wang, J. & Ma, Y. Effects of beta-adrenergic antagonist, propranolol on spatial memory and exploratory behavior in mice. *Neuroscience letters* **498**, 133-137, doi:10.1016/j.neulet.2011.04.076 (2011).

75 Catus, S. L., Gibbs, M. E., Sato, M., Summers, R. J. & Hutchinson, D. S. Role of beta-adrenoceptors in glucose uptake in astrocytes using beta-adrenoceptor knockout mice. *British journal of pharmacology* **162**, 1700-1715, doi:10.1111/j.1476-5381.2010.01153.x (2011).

76 Dong, J. H. *et al.* beta2-adrenergic receptor and astrocyte glucose metabolism. *J Mol Neurosci* **48**, 456-463, doi:10.1007/s12031-012-9742-4 (2012).

77 Bittner, C. X. *et al.* Fast and reversible stimulation of astrocytic glycolysis by K+ and a delayed and persistent effect of glutamate. *The Journal of neuroscience : the official journal of the Society for Neuroscience* **31**, 4709-4713, doi:10.1523/JNEUROSCI.5311-10.2011 (2011).

78 Ruminot, I. *et al.* NBCe1 mediates the acute stimulation of astrocytic glycolysis by extracellular K+. *The Journal of neuroscience : the official journal of the Society for Neuroscience* **31**, 14264-14271, doi:10.1523/JNEUROSCI.2310-11.2011 (2011).

79 Brown, A. M. & Ransom, B. R. Astrocyte glycogen and brain energy metabolism. *Glia* **55**, 1263-1271, doi:10.1002/glia.20557 (2007).

80 Obel, L. F. *et al.* Brain glycogen-new perspectives on its metabolic function and regulation at the subcellular level. *Frontiers in neuroenergetics* **4**, 3, doi:10.3389/fnene.2012.00003 (2012).

81 Savaki, H. E., Kadekaro, M., Jehle, J. & Sokoloff, L. α- And β-adrenoreceptor blockers have opposite effects on energy metabolism of the central auditory system. *Nature* **276**, 521-523, doi:10.1038/276521a0 (1978).

82 Mayrhofer, J. M., Haiss, F., Helmchen, F. & Weber, B. Sparse, reliable, and long-term stable representation of periodic whisker deflections in the mouse barrel cortex. *NeuroImage* **115**, 52-63, doi:10.1016/j.neuroimage.2015.04.045 (2015).

83 Mayrhofer, J. M. *et al.* Novel two-alternative forced choice paradigm for bilateral vibrotactile whisker frequency discrimination in head-fixed mice and rats. *Journal of neurophysiology* **109**, 273-284, doi:10.1152/jn.00488.2012 (2013).

84 Mayrhofer, J. M. *et al.* Design and performance of an ultra-flexible two-photon microscope for in vivo research. *Biomed Opt Express* **6**, 4228-4237, doi:10.1364/BOE.6.004228 (2015).

85 Pologruto, T. A., Sabatini, B. L. & Svoboda, K. ScanImage: flexible software for operating laser scanning microscopes. *Biomedical engineering online* **2**, 13, doi:10.1186/1475-925X-2-13 (2003).

86 Schneider, C. A., Rasband, W. S. & Eliceiri, K. W. NIH Image to ImageJ: 25 years of image analysis. *Nature methods* **9**, 671-675 (2012).

87 Bates, D., Machler, M., Bolker, B. M. & Walker, S. C. Fitting Linear Mixed-Effects Models Using lme4. *J Stat Softw* **67**, 1-48, doi:10.18637/jss.v067.i01 (2015).

88 Hothorn, T., Bretz, F. & Westfall, P. Simultaneous inference in general parametric models. *Biometrical journal. Biometrische Zeitschrift* **50**, 346-363, doi:10.1002/bimj.200810425 (2008).

Figure legends

Figure 1. Awake two-photon imaging to study cortical lactate and calcium dynamics in neurons and astrocytes.

(A) Animals were trained for head-restrained, awake two-photon imaging. A water spout was used for reward delivery and a ventilation mask for isoflurane supply. **(B)** Workflow scheme of preparing mice for awake two-photon imaging. Following recovery from surgery and intracortical AAV injections, mice were trained for head-restrained imaging using a suppression-response task and a water reward. On average mice were ready for imaging at around 4 weeks after surgery. **(C)** Mean behavioral performance (gray) and learning progress (black) during training. On average mice performed 139 ± 33 trials per session and 2835 ± 1320 total trials to reach the 75% performance criterion to be included for imaging. N = number of animals, n = number of sessions. **(D)** Cortical expression of genetically-encoded lactate sensor Laconic [34], calcium sensor RCaMP 1.07 [35] and GCaMP6s [36] imaged through a chronic cranial window. M = medial, L = lateral, C = cranial, R = rostral. **(E)** Representative images of Laconic expression in neurons (blue), Laconic in astrocytes (yellow), RCaMP 1.07 in neurons (red) and GCaMP6s in astrocytes (green) 100-200 µm below cortical surface. Fluorescence is given in pseudo-colors.

Figure 2. Arousal-induced calcium and lactate elevations in neurons and astrocytes.

(A) Paradigm to induce arousal in awake mice, consisting of a 5 min baseline (awake), 20 s isoflurane exposure (ISO pulse) and a 14 min and 40 s post-stimulation period. **(B)** Brief ISO pulse induces pupil dilation (T5.2) without a subsequent miosis, as expected for an arousal response. White circles indicate pupil size approximation. **(C, D)** Neurons (C) and astrocytes (D) immediately respond with an increase in calcium (T5.2) upon ISO pulse. Relative calcium changes normalized to baseline are quantified at timepoints T2, T5.2, T7 and T20 (bar graphs). The timepoint of isoflurane onset (T5) is indicated by ISO. **(E, F)** Depicted are lactate level changes in neurons (E) and astrocytes (F). Arousal induces lactate level elevations in both cell types (T7). Note that only astrocytes reveal a significant dip in lactate levels immediately after ISO pulse (T5.2). Quantification of relative lactate level changes at timepoints T2,

T5.2, T7 and T20 (bar graphs). Data set comprises 226 neurons and 236 astrocytes. **(G, H)** Overlay of calcium (black) and lactate responses (red) in neurons (G) and astrocytes (H). Note that in astrocytes the evoked calcium response strongly coincides with the immediate, initial drop in lactate levels. Dashed lines are indicated for slope analysis (I). **(I)** Response slopes of the evoked lactate rise. Astrocytes revealed a faster lactate level rise compared to neurons (8.3 ± 1.1 %/min vs. 4.7 ± 3.3 %/min; $p < 0.001$). N = number of animals, n = number of experiments. Data is represented as mean ± SD (* = $p < 0.05$; ** = $p < 0.01$; *** = $p < 0.001$; Tukey post-hoc test).

Figure 3. Lactate response kinetics suggest an activity-dependent release of lactate from astrocytes upon arousal.

(A) Scheme of extracellular space (ECS) lactate recordings using a pre-calibrated Pinnacle lactate biosensor inserted into the somatosensory cortex. **(B)** ECS lactate level changes in response to arousal (ISO pulse). Note that the ECS lactate surge has two distinct slopes (S1 and S2) indicated by dashed red lines. **(C)** Quantification of ECS lactate surge at timepoints T5.2 and T7 (318.2 ± 60.7 µM and 1099.3 ± 145.9 µM) and of the slopes S1 and S2 (25.8 ± 6.3 µM/s and 8.1 ± 3.8 µM/s). **(D)** For direct comparison of the arousal-evoked lactate responses of the three compartments: ECS data using a Pinnacle biosensor (B), astrocytes and neurons using Laconic (reproduced from Figure 3E and F). Data was binned into 12 s fragments for data visibility. Green section of curves indicates the first 60 s upon arousal (ISO pulse). T5.2 represents the first datapoint 12 s after ISO pulse. **(E)** Normalized lactate responses from astrocytes, neurons and ECS. Green shaded area indicates first 60 s upon ISO pulse. Note that the astrocyte lactate level dip coincides with the lactate level rise in ECS, whereas neuronal lactate levels follow the rise in ECS. **(F)** Magnification of the time course depicted in (E) to better visualize lactate response kinetics. Green shaded area indicates first 60 s upon ISO pulse and gray shaded area indicates margins of 2 times standard deviations (SD) of the baseline of all 3 recordings. Two distinct phases are highlighted. First phase (I): Lactate level drop in astrocytes parallels rise in the ECS; Second phase (II): Neuronal lactate rise slows down ECS lactate surge. **(G-I)** Time series comparison of normalized data from E between neuronal, astrocytic and ECS responses. Overall strong

positive linear relationship (R) between neurons, astrocytes and ECS. Scatter plots reveal distinct temporal kinetics within first 60 s of arousal (green dots and line). Red line indicates identity line and a correlation of 1. **(G)** Direct comparison of ECS with astrocytes upon arousal (T5.2 onwards) shows a decrease in association, a significant left shift from the identity line (red), in favor of ECS lactate increases, as revealed by the distribution of datapoints in the histogram. **(H)** ECS vs. neuron comparison displays similar kinetics to the ECS vs. astrocyte comparison with significant outliers and a left shift from the identity line towards ECS coordinate during arousal. **(I)** Comparing neurons to astrocytes shows a decrease in value proximity during the first minute after stimulation onset and a significant right shift of the values from the identity line (red line = correlation of 1) as revealed by the distribution histogram due to the pronounced decrease in astrocytic lactate. Overall comparison reveals that ECS shows the fastest increase in lactate levels followed by astrocytes and neurons. ECS and neurons show no negative transients and only astrocytes show a dip. After arousal, response values return to the identity line and a linear relationship. Histogram showing data distribution compared to identity line and statistical analysis of differences between compartments (* = $p < 0.05$; ** = $p < 0.01$; *** = $p < 0.001$, T-test). Arrow indicates first datapoint after ISO pulse (T5.2). Correlation (R) was computed with Pearson's linear correlation coefficient at a significance level of 0.05. Data sets were normalized to 0 (baseline) and 1 (maximal response) for comparison.

Figure 4. β-adrenergic signaling mediates arousal-evoked lactate surges.

(A) Scheme to investigate propranolol (β-adrenergic antagonist) effects on arousal-induced lactate responses. Propranolol (10 mg/kg, i.p.) was injected after baseline acquisition (0 h). The same cells were imaged in subsequent sessions 1, 3, 6 and 24 h after the injection. **(B, C)** Evoked lactate response in neurons (B) and astrocytes (C) before (0 h) and after propranolol injection (1, 3, 6 and 24 h). The same 113 neurons and 118 astrocytes were monitored in 6 independent experiments per timepoint. **(D)** Quantification of the area under the curve (AUC) of the evoked lactate dip in astrocytes before (0 h) and after propranolol (1 h - 24 h). The isoflurane-induced dip in astrocytes was not overtly affected by propranolol. **(E)** Arousal-induced lactate surges (AUC) in neurons (left) and astrocytes (right) before

(0 h) and after propranolol injection (1 h - 24 h). Blocking β-receptors resulted in a gradual decrease of the AUC in neurons and astrocytes. Maximal decreases were measured 6 h after propranolol injection (neurons: from 4.9 ± 3.3 %×min to 2.5 ± 2.0 %×min; $p < 0.001$; and astrocytes: from 7.3 ± 5.1 %×min to 5.0 ± 3.4 %×min; $p < 0.001$). Responses recovered within 24 h after propranolol injection. **(F)** Quantification of response slopes in neurons (left) and astrocytes (right) before and after propranolol injection (0 h - 24 h). By 1 h after injection, slopes were already decreased. 6 h after injection neuronal response decreased from 5.5 ± 3.2 %/min to 3.6 ± 2.3 %/min ($p < 0.001$) and astrocyte response decreased from 7.9 ± 6.6 %/min to 5.1 ± 4.9 %/min ($p = 0.004$). Response slopes recovered within 24 h. N = number of animals, n = experiments. Data is represented as mean ± SD (* = $p < 0.05$; ** = $p < 0.01$; *** = $p < 0.001$, Tukey post-hoc test).

Figure 5. Model of arousal-induced lactate mobilization from astrocytes.

Arousal-induced cortical activity triggers an immediate lactate release from the astrocytic "pressure reservoir" [65]. The gray shaded area represents steady-state lactate levels in all three compartments and highlights the lactate gradient from astrocytes to neurons [17]. The activity-evoked drop in astrocytic lactate is paralleled by a rapid rise in extracellular lactate levels (I, red). This initial astrocytic lactate release is most likely driven by cellular depolarization and a rise in extracellular [K+] [13]. Moreover, arousal induces release of noradrenaline (NA) that activates β-adrenergic receptors on astrocytes. β-adrenergic signaling stimulates glycogenolysis in astrocytes, thereby promoting additional lactate production and release (II, blue). Neurons increase their lactate levels most likely by uptake of lactate, thereby slowing down the astrocyte-mediated extracellular lactate surge (II, blue). Neurons may already take up lactate in the initial phase (I, red) which may be directly used to fuel cellular activity (arousal-evoked calcium transients; Fig. 2) resulting in balanced uptake and consumption. Neuronal depolarization may also stimulate glycolysis in neurons, which may also contribute to the neuronal lactate rise [18].

Figure 1

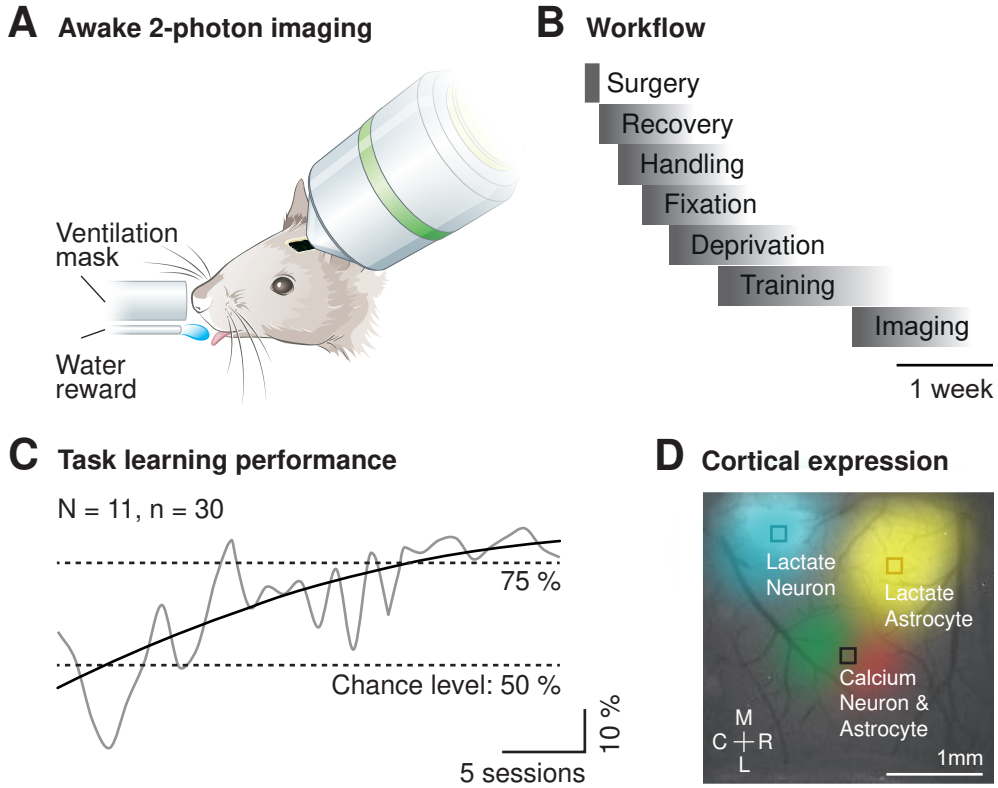
A
Awake 2-photon imaging
Ventilation mask
Water reward
B
Workflow
Surgery
Recovery
Handling
Fixation
Deprivation
Training
Imaging
1 week
C
Task learning performance
N = 11, n = 30
75 %
Chance level: 50 %
10 %
5 sessions
D
Cortical expression
Lactate Neuron
Lactate Astrocyte
Calcium Neuron & Astrocyte
M
C R
L
1mm
E
Cellular expression
Laconic Neurons
Laconic Astrocytes
RCaMP 1.07 Neurons
GCaMP6s Astrocytes
100 µm

Figure 2

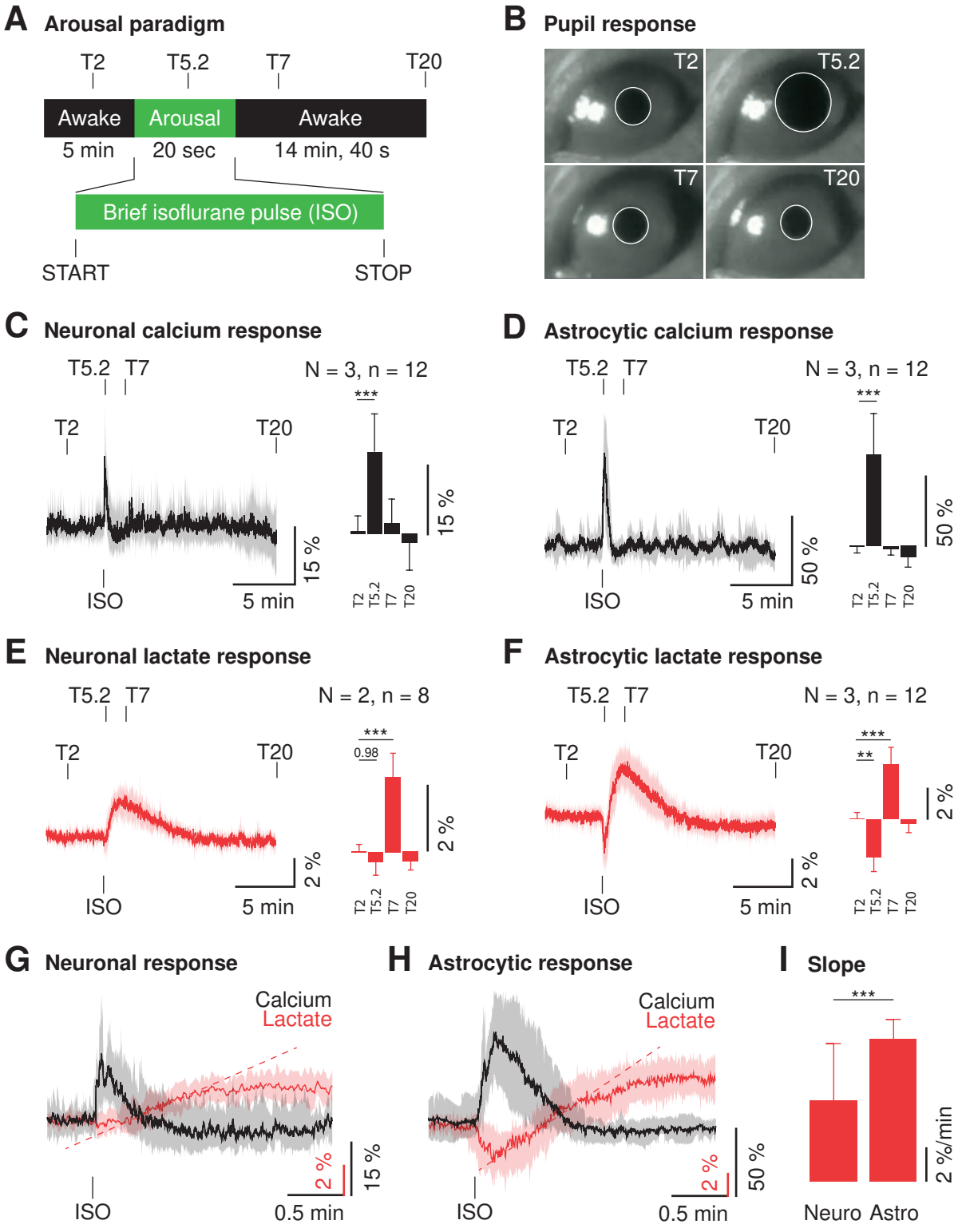
A
Arousal paradigm
T2
T5.2
T7
T20
Awake
Arousal
Awake
5 min
20 sec
14 min, 40 s
Brief isoflurane pulse (ISO)
START
STOP
B
Pupil response
T2
T5.2
T7
T20
C
Neuronal calcium response
T5.2 T7
N = 3, n = 12
T2
T20
***
15 %
ISO
5 min
15 %
T2 T5.2 T7 T20
D
Astrocytic calcium response
T5.2 T7
N = 3, n = 12
T2
T20
***
50 %
ISO
5 min
50 %
T2 T5.2 T7 T20
E
Neuronal lactate response
T5.2 T7
N = 2, n = 8
T2
T20
***
0.98
2 %
ISO
5 min
2 %
T2 T5.2 T7 T20
F
Astrocytic lactate response
T5.2 T7
N = 3, n = 12
T2
T20
***
**
2 %
ISO
5 min
2 %
T2 T5.2 T7 T20
G
Neuronal response
Calcium
Lactate
2 %
15 %
ISO
0.5 min
H
Astrocytic response
Calcium
Lactate
2 %
50 %
ISO
0.5 min
I
Slope
***
2 %/min
Neuro Astro

Figure 3

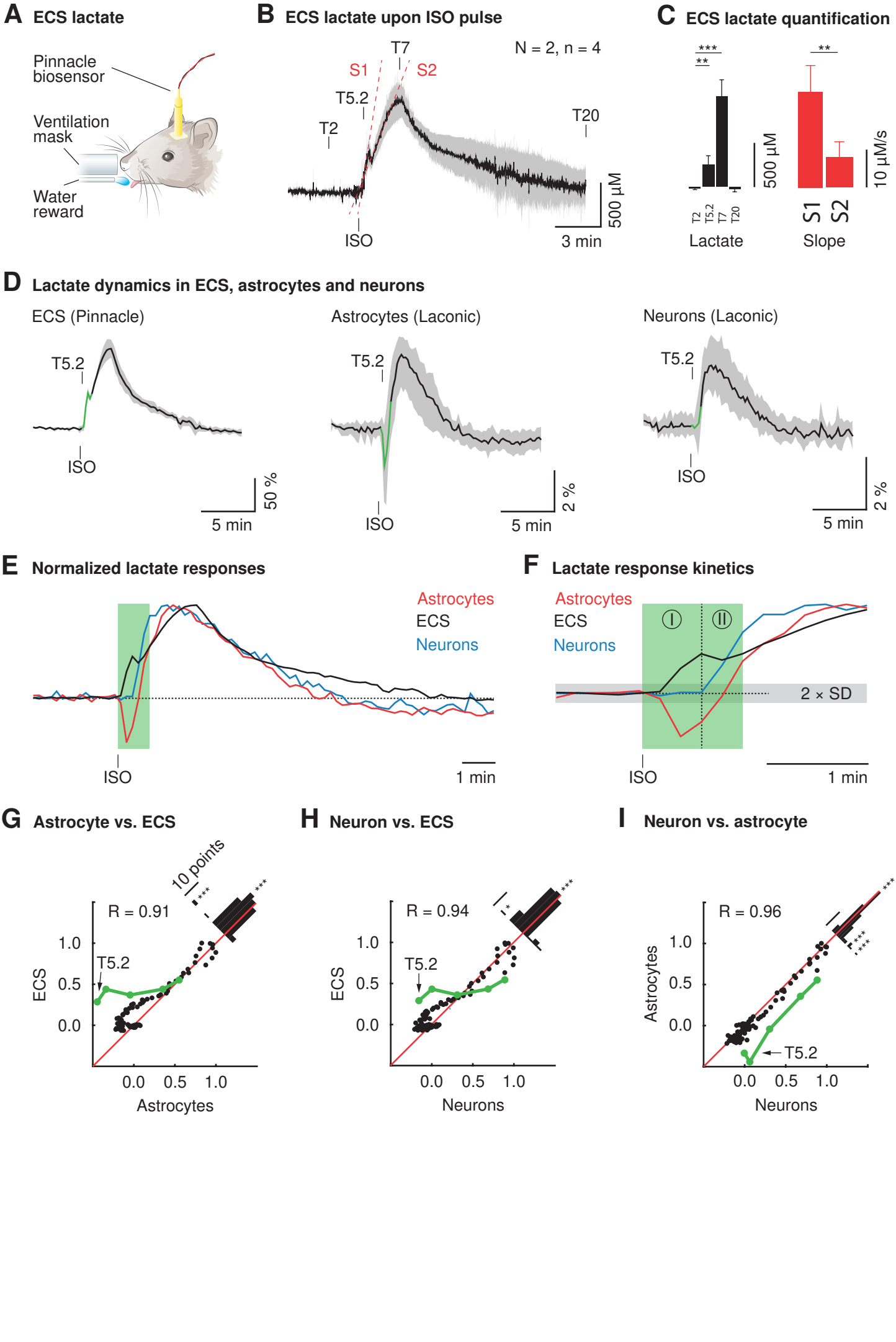
A ECS lactate
Pinnacle biosensor
Ventilation mask
Water reward
B ECS lactate upon ISO pulse
N = 2, n = 4
T7
S1
S2
T5.2
T2
T20
ISO
500 µM
3 min
C ECS lactate quantification
***
**
**
500 µM
10 µM/s
T2
T5.2
T7
T20
S1
S2
Lactate
Slope
D Lactate dynamics in ECS, astrocytes and neurons
ECS (Pinnacle)
Astrocytes (Laconic)
Neurons (Laconic)
T5.2
ISO
50 %
2 %
5 min
E Normalized lactate responses
Astrocytes
ECS
Neurons
ISO
1 min
F Lactate response kinetics
Astrocytes
ECS
Neurons
I
II
2 × SD
ISO
1 min
G Astrocyte vs. ECS
10 points
R = 0.91
T5.2
ECS
Astrocytes
H Neuron vs. ECS
R = 0.94
T5.2
ECS
Neurons
I Neuron vs. astrocyte
R = 0.96
T5.2
Astrocytes
Neurons

Figure 4

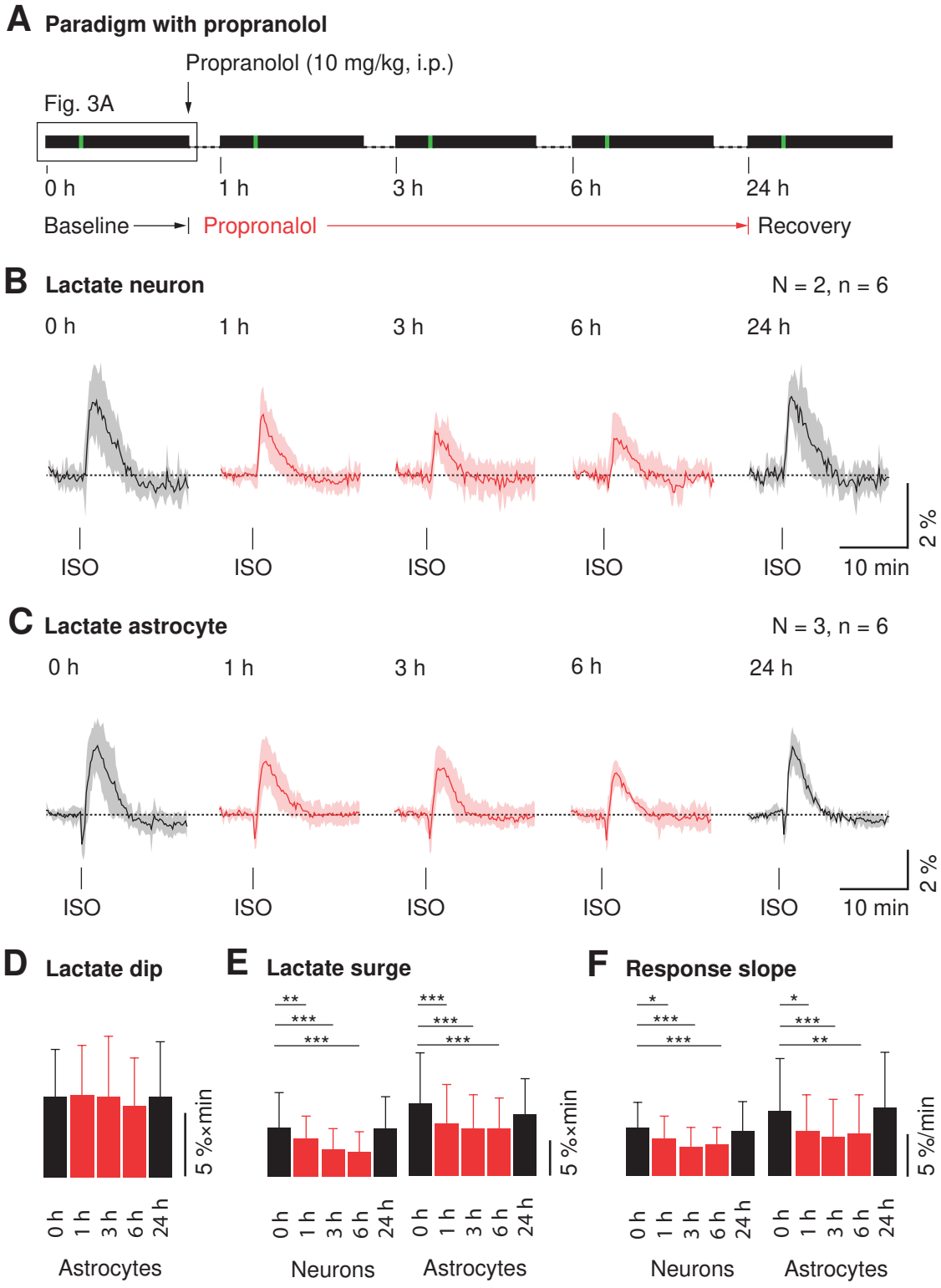
A
Paradigm with propranolol
Propranolol (10 mg/kg, i.p.)
Fig. 3A
0 h
1 h
3 h
6 h
24 h
Baseline
Propronalol
Recovery
B
Lactate neuron
N = 2, n = 6
0 h
1 h
3 h
6 h
24 h
ISO
ISO
ISO
ISO
ISO
10 min
2 %
C
Lactate astrocyte
N = 3, n = 6
0 h
1 h
3 h
6 h
24 h
ISO
ISO
ISO
ISO
ISO
10 min
2 %
D
Lactate dip
5 %×min
0 h
1 h
3 h
6 h
24 h
Astrocytes
E
Lactate surge
**
***
***
***
***
***
5 %×min
0 h
1 h
3 h
6 h
24 h
Neurons
0 h
1 h
3 h
6 h
24 h
Astrocytes
F
Response slope
*
***
***
*
***
**
5 %/min
0 h
1 h
3 h
6 h
24 h
Neurons
0 h
1 h
3 h
6 h
24 h
Astrocytes

Figure 4

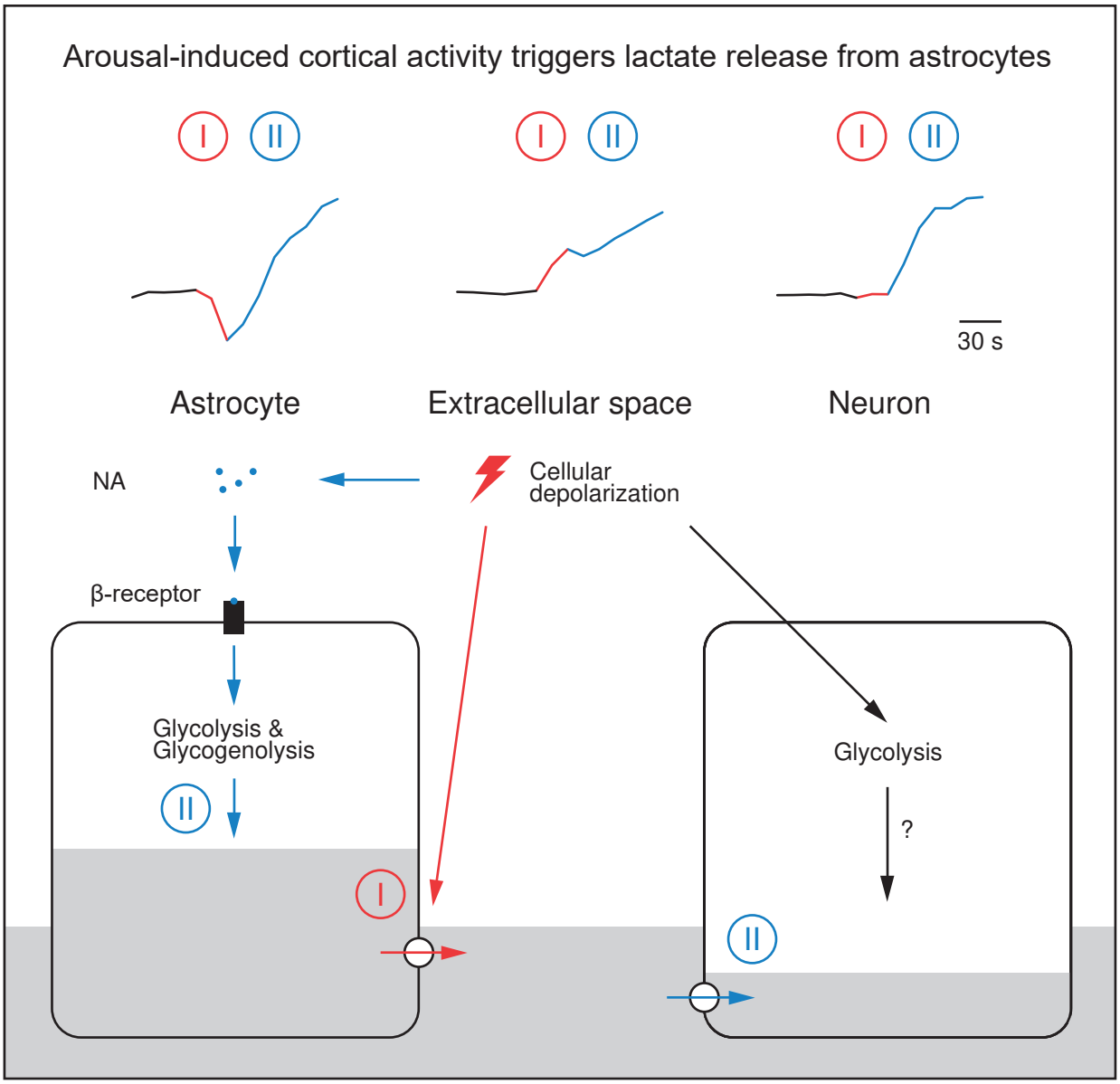
Arousal-induced cortical activity triggers lactate release from astrocytes
I
II
30 s
Astrocyte
Extracellular space
Neuron
NA
Cellular depolarization
β-receptor
Glycolysis & Glycogenolysis
Glycolysis
?

1 **Supplemental information**

2 **Supplemental figures**

Figure S1. Lactate dynamics in cortical neurons and astrocytes upon acute isoflurane exposure. (Related to Figure 2)

(A) Scheme of the prolonged isoflurane imaging paradigm consisting of a 10 min baseline (awake behaving), 20 min isoflurane and a 30 min recovery period. T indicates time in min throughout the imaging session. Timepoints for the onset (T10) and end (T30) of isoflurane delivery are indicated by START and STOP. **(B, C)** Cortical neurons (B, left panel) and astrocytes expressing Laconic (C, left panel) in individual fields of view. Single-cell fluorescence analysis of relative lactate changes (middle panels) during the isoflurane administration protocol (A). Both neurons and astrocytes show a rise in lactate levels that persists during the isoflurane period (indicated at T30) and returns to baseline during recovery (indicated at T60). Note, astrocytes revealed a significant lactate level drop shortly after isoflurane onset (C, indicated at T10.2). Bar graphs (right) summarize relative changes at T5, T10.2, T30 and T60. N = number of animals, N = number of experiments. Data is represented as mean ± SD (* = $p < 0.05$; ** = $p < 0.01$; *** = $p < 0.001$, Tukey post-hoc test).

Figure S2. Isoflurane exposure causes an initial arousal response before reaching the anesthetized state. (Related to Figure 2)

(A) EEG raw traces at different timepoints of the isoflurane imaging paradigm (Figure S1A). Traces represent distinct states such as: T5 = awake behaving, T10.2 = induction and desynchronization, T30 = anesthetized and increased slow-wave activity leading to burst suppression, T60 = recovery and awake. **(B)** EEG spectrum and EEG bands (delta: 0.5-4 Hz, theta: 4-8 Hz, alpha: 8-12 Hz, beta: 12-30 Hz and gamma: 30-50 Hz) show a clear shift in the power spectrum upon isoflurane exposure. Blue = low power (30 dB) and red = high power (90 dB). **(C)** EEG bands according to their power display a biphasic EEG response when transiting from the awake state through the induction phase (increase in high-frequency power) to the anesthetized state (increase in low-frequency power). **(D)** Quantification of EEG bands as a relative change with respect to baseline at timepoints T5, T10.2, T30 and T60. During the initial induction phase (T10.2) high-frequency bands (gamma, beta) significantly increased whereas in the anesthetized state (T30) spectral power shifted to low-frequency bands. **(E)** EMG spectrum (10-30 Hz) recorded from neck muscles shows an increase in muscle activity with exposure to isoflurane and a reduced power in the anesthetized state. Blue = low power (30 dB) and red = high power (90 dB). **(F)** Pupillometry analysis reveals a pupil dilation in the induction phase (T10.2), then a pupil constriction in the anesthetized state (T30). White circles indicate approximate pupil sizes. **(G)** Relative changes in EMG power (black) and pupil radius (red) recorded during the isoflurane paradigm. **(H)** Quantification of EMG and pupil radius at timepoints T5, T10.2, T30 and T60. Note a significant increase in neuromuscular activity in the induction phase and a reduction in EMG power and pupil size during the anesthetized state. **(I)** Summary scheme highlighting that acute isoflurane exposure first initiates an aroused state (within the first 60 s), which is then gradually followed by an anesthetized state as determined by the EEG, EMG and pupil size analyses. N = number of animals, n = number of experiments. START and STOP indicate the period of isoflurane administration. Data is represented as mean ± SD (* = $p < 0.05$; ** = $p < 0.01$; *** = $p < 0.001$; Tukey post-hoc test).

Figure S3. Calcium activity in neurons and astrocytes upon isoflurane administration. (Related to Figure 2)

(A) Scheme of the prolonged isoflurane imaging paradigm consisting of a 10 min baseline (awake behaving), 20 min isoflurane and a 30 min recovery period. T indicates time in min for the course of the imaging session. Timepoints for the onset (T10) and end (T30) of isoflurane delivery are indicated by START and STOP. **(B, C)** Cortical neurons expressing calcium sensor RCaMP 1.07 (B, left panel) and astrocytes expressing GCaMP6s (C, left panel) in same field of view and spectrally separated. Whole frame fluorescence analysis of relative calcium changes (middle panels) during the isoflurane administration paradigm (A). The onset of isoflurane exposure (START) caused a strong activation in cortical network and a significant rise in neuronal and astrocytic calcium levels (T10.2). Overall calcium levels decreased in both cell types during the anesthetized state (T30) and recovered to baseline levels when mice returned to the awake state (T60). Bar graphs on the right summarize calcium level changes at timepoints T5, T10.2, T30 and T60. **(D, E)** Automated analysis to identify calcium events for neurons (D) and astrocytes (E) using MATLAB toolbox CHIPS (Barrett et al., 2018). Detected signals are indicated by colored ROI masks for timepoints T5, T10.2, T30 and T60 of the isoflurane administration paradigm (A). Quantification of the number of events detected during these timepoints are summarized in bar graphs (right). With isoflurane administration there is a significant increase in calcium events in both neurons and astrocytes (T10.2) compared to baseline (T5). Event frequencies are strongly reduced during the anesthetized state (T30) and recover back to baseline at T60. N = number of animals, N = number of experiments. ROI = region of interest. Data is represented as mean ± SD (* = $p < 0.05$; ** = $p < 0.01$; *** = $p < 0.001$, Tukey post-hoc test).

Figure S4. Accurate recurring imaging allows repetitive monitoring of the same cortical neurons and astrocytes. (Related to Figure 4)

(A-D) Repeated imaging of the same neurons and astrocytes over several timepoints (0, 1, 3, 6 and 24 h; from left to right) for calcium (A, C) and lactate (B, D) measurements as used for the propranolol paradigm (Figure 4A). Similarity of field of views are given as correlation coefficients (R; top right) when compared to the first image of baseline acquisition (0 h). Correlation was computed with MATLAB toolbox CHIPS (Barrett et al., 2018). h indicates time in hours after starting the propranolol paradigm.

Figure S5. Arousal-evoked calcium responses in neurons and astrocytes were unperturbed with propranolol. (Related to Figure 4)

(A) Scheme of the paradigm used to investigate the effects of propranolol in neurons and astrocytes. Propranolol (10mg/kg, i.p.) was injected after baseline acquisition (0 h) and the same cells were imaged in subsequent sessions 1, 3, 6 and 24 h after injection. **(B-E)** Isoflurane pulse-evoked calcium changes in neurons (B, C) and astrocytes (D, E) at different timepoints before (0 h) and after propranolol injection (1, 3, 6 and 24 h). The evoked neuronal and astrocytic calcium responses (whole frame analysis) did not significantly change with propranolol treatment and signal amplitudes did not differ from control experiments with saline injections (Figure S4). N = number of animals, n = number experiments. ISO indicates the start of 20 s isoflurane application. Data is represented as mean ± SD.

Figure S6. Control saline experiments of calcium and lactate responses in neurons and astrocytes. (Related to Figure 4)

(A) Scheme of the control paradigm with saline for arousal-induced calcium and lactate responses in neurons and astrocytes (Figure 4A). The same cells as in the propranolol paradigm were monitored in sequential imaging sessions. **(B, D)** Evoked calcium responses in neurons (B) and astrocytes (D) before (0 h) and after saline injection (1 h - 24 h). **(C, E)** Quantification of the amplitude of the evoked calcium responses in neurons (C) and astrocytes (E) before and after saline (0 h - 24 h). The isoflurane-induced calcium responses in neurons and astrocytes were not affected by saline injection. **(F, H)** Evoked lactate response in neurons (F) and astrocytes (H) before and after saline injection (0 h - 24 h). **(G, I)** Quantification of the AUC of the evoked lactate surge in neurons (G) and astrocytes (I) before and after saline injection (0 h - 24 h). The isoflurane-induced lactate response in neurons and astrocytes was not affected by saline injection. Data is represented as mean ± SD. AUC = area under the curve. N = number of animals, n = number of experiments.

Figure S1

A **Imaging paradigm**

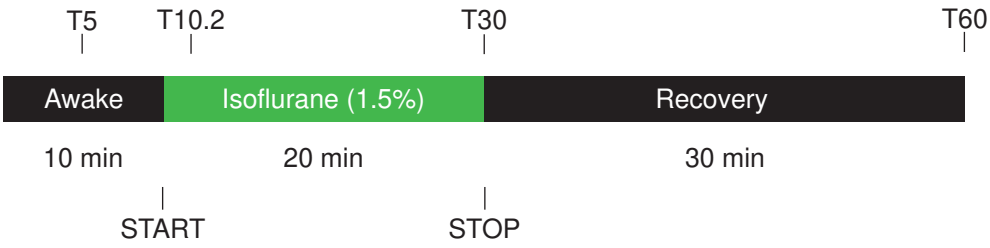

B **Whole frame fluorescence in neurons**

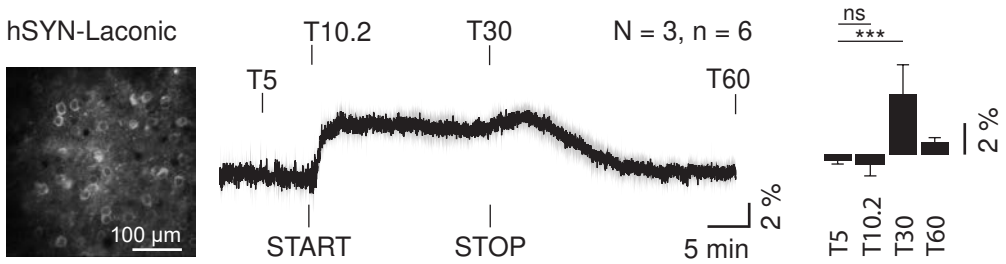

C **Whole frame fluorescence in astrocytes**

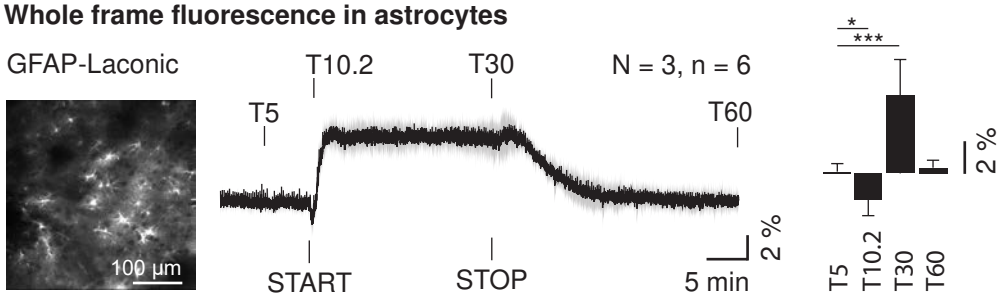

Figure S2

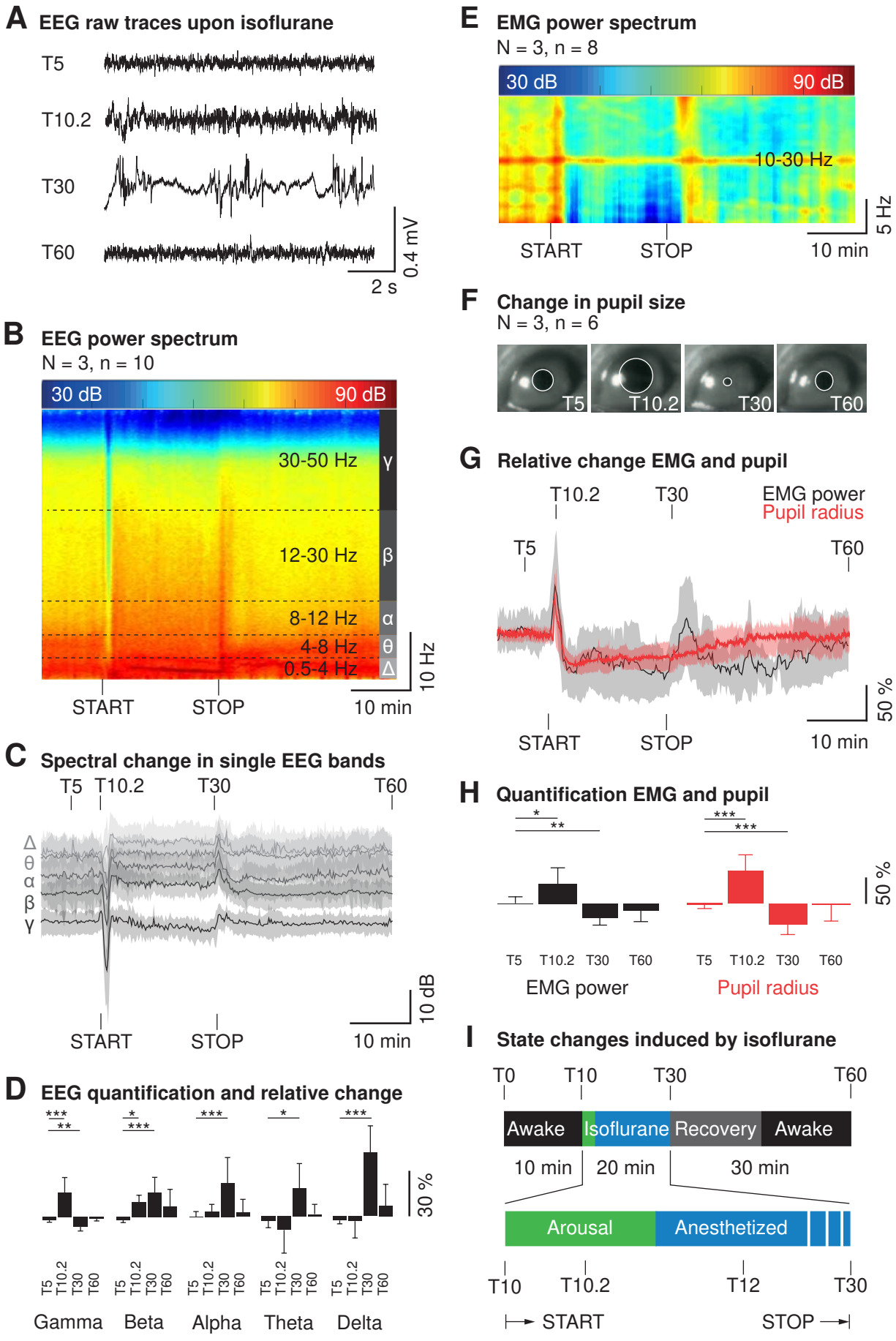
A
EEG raw traces upon isoflurane
T5
T10.2
T30
T60
0.4 mV
2 s
B
EEG power spectrum
N = 3, n = 10
30 dB
90 dB
30-50 Hz
γ
12-30 Hz
β
8-12 Hz
α
4-8 Hz
θ
0.5-4 Hz
Δ
10 Hz
START
STOP
10 min
C
Spectral change in single EEG bands
T5
T10.2
T30
T60
Δ
θ
α
β
γ
START
STOP
10 min
10 dB
D
EEG quantification and relative change
30 %
T5 T10.2 T30 T60
Gamma
Beta
Alpha
Theta
Delta
E
EMG power spectrum
N = 3, n = 8
30 dB
90 dB
10-30 Hz
5 Hz
START
STOP
10 min
F
Change in pupil size
N = 3, n = 6
T5
T10.2
T30
T60
G
Relative change EMG and pupil
T10.2
T30
EMG power
Pupil radius
T5
T60
START
STOP
10 min
50 %
H
Quantification EMG and pupil
50 %
T5 T10.2 T30 T60
EMG power
Pupil radius
I
State changes induced by isoflurane
T0
T10
T30
T60
Awake
Isoflurane
Recovery
Awake
10 min
20 min
30 min
Arousal
Anesthetized
T10
T10.2
T12
T30
START
STOP

Figure S3

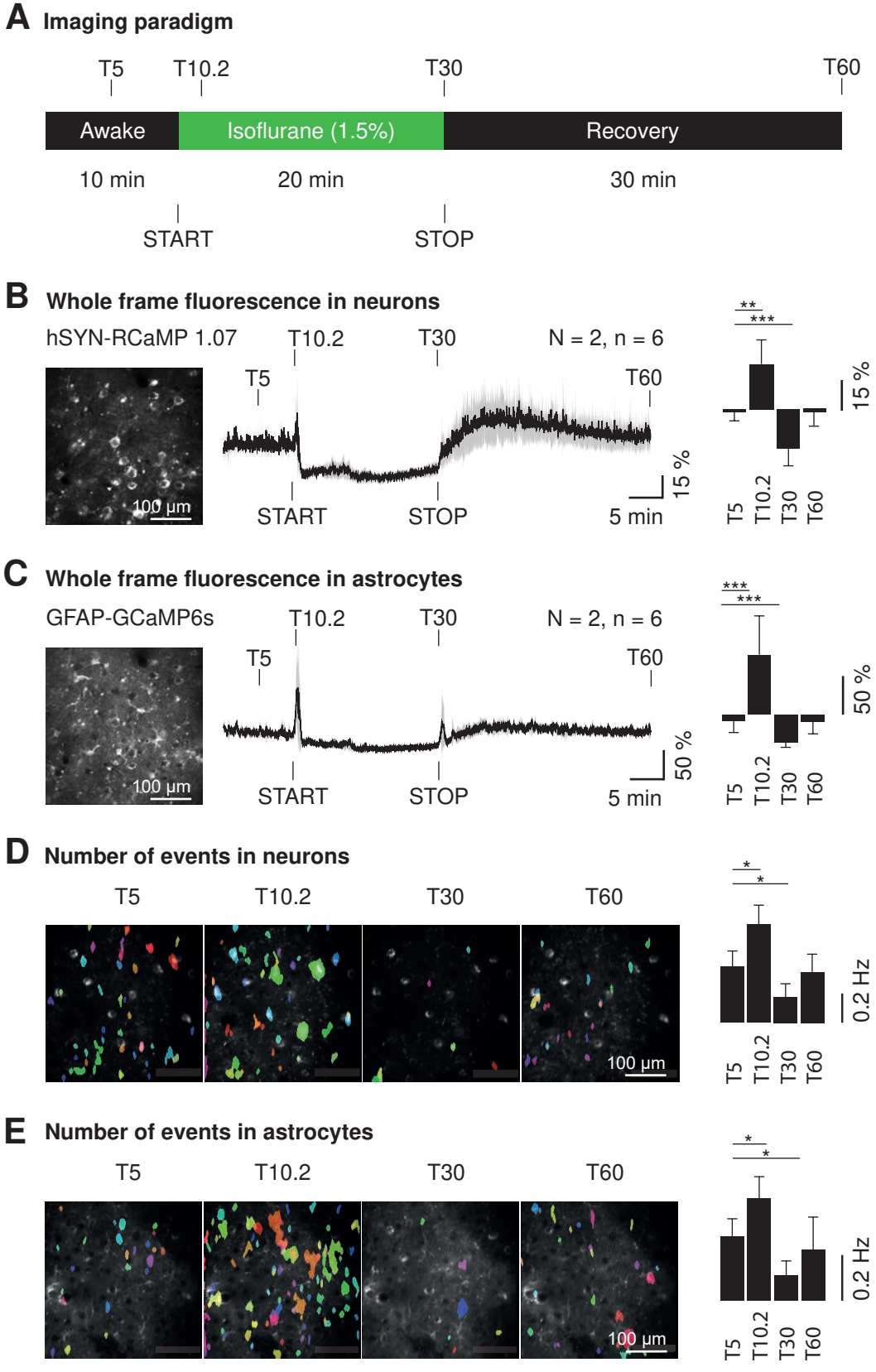
A
Imaging paradigm
T5
T10.2
T30
T60
Awake
Isoflurane (1.5%)
Recovery
10 min
20 min
30 min
START
STOP
B
Whole frame fluorescence in neurons
hSYN-RCaMP 1.07
T10.2
T30
N = 2, n = 6
T5
T60
100 µm
START
STOP
5 min
15 %
**
***
15 %
T5
T10.2
T30
T60
C
Whole frame fluorescence in astrocytes
GFAP-GCaMP6s
T10.2
T30
N = 2, n = 6
T5
T60
100 µm
START
STOP
5 min
50 %
***
***
50 %
T5
T10.2
T30
T60
D
Number of events in neurons
T5
T10.2
T30
T60
100 µm
*
*
0.2 Hz
T5
T10.2
T30
T60
E
Number of events in astrocytes
T5
T10.2
T30
T60
100 µm
*
*
0.2 Hz
T5
T10.2
T30
T60

Figure S4

A **RCaMP 1.07 in neurons**

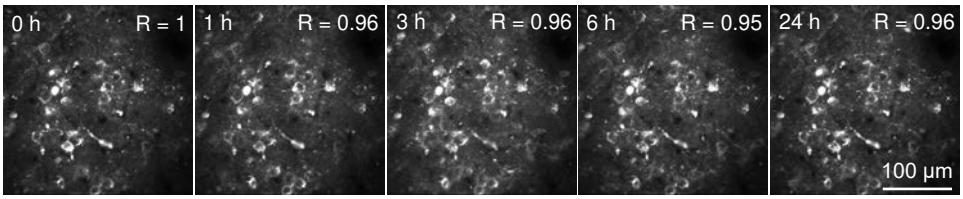

B **Laconic in neurons**

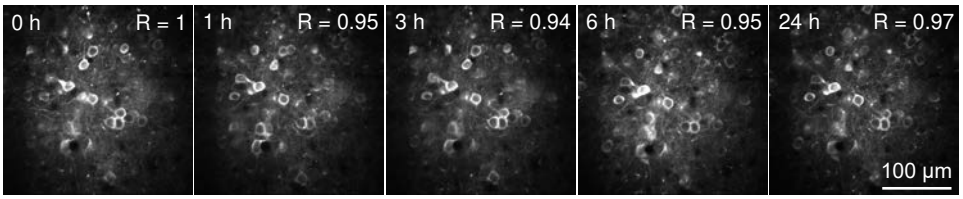

C **GCaMP6s in astrocytes**

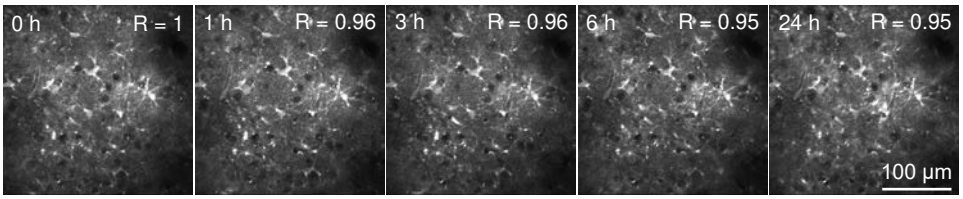

D **Laconic in astrocytes**

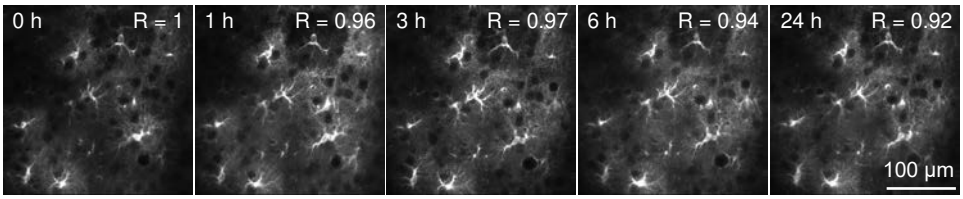

Figure S5

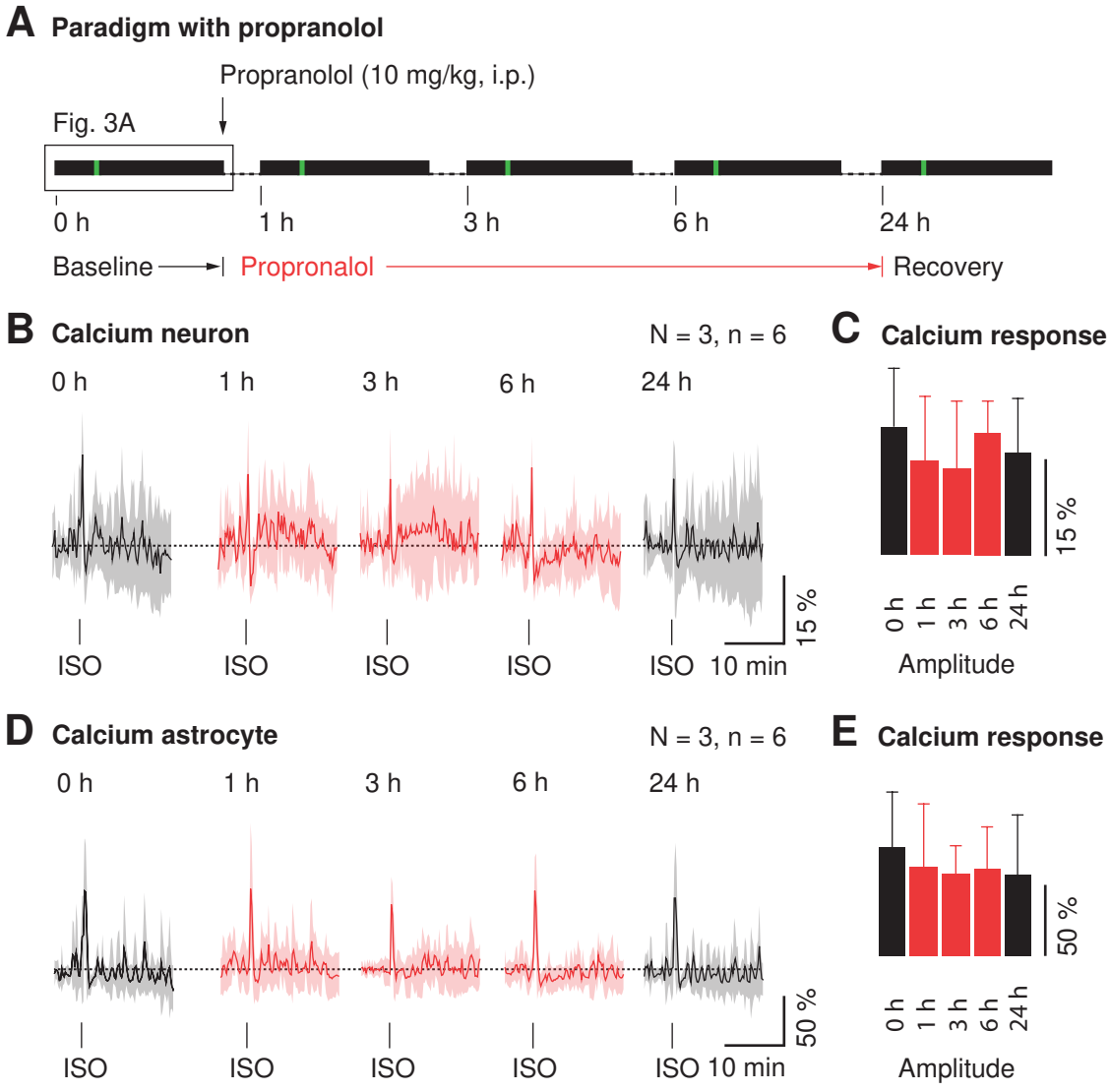
A
Paradigm with propranolol
Propranolol (10 mg/kg, i.p.)
Fig. 3A
0 h
1 h
3 h
6 h
24 h
Baseline
Propronalol
Recovery
B
Calcium neuron
N = 3, n = 6
0 h
1 h
3 h
6 h
24 h
ISO
ISO
ISO
ISO
ISO
10 min
15 %
C
Calcium response
15 %
0 h
1 h
3 h
6 h
24 h
Amplitude
D
Calcium astrocyte
N = 3, n = 6
0 h
1 h
3 h
6 h
24 h
ISO
ISO
ISO
ISO
ISO
10 min
50 %
E
Calcium response
50 %
0 h
1 h
3 h
6 h
24 h
Amplitude

Figure S6

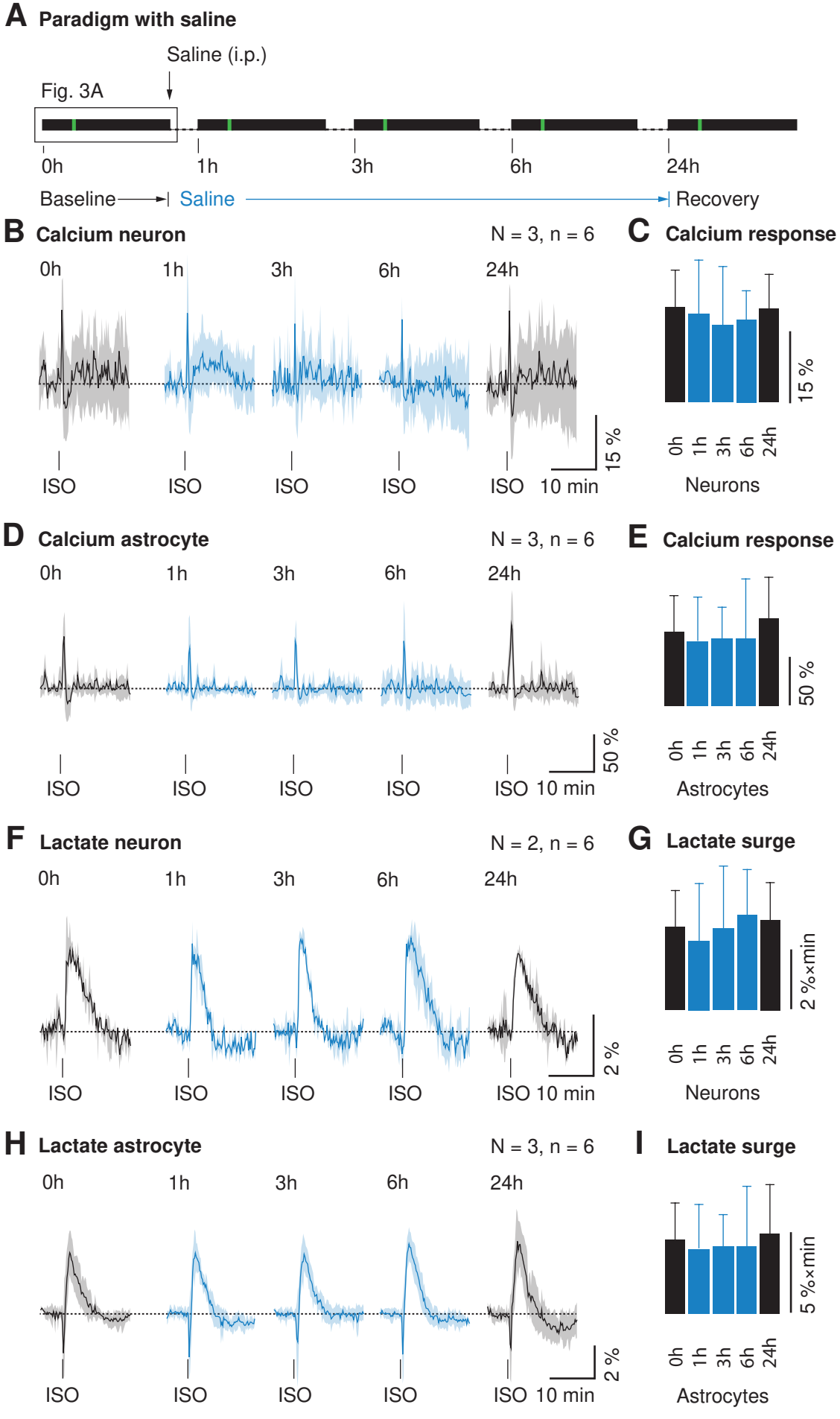
A Paradigm with saline
Saline (i.p.)
Fig. 3A
0h
1h
3h
6h
24h
Baseline
Saline
Recovery
B Calcium neuron
N = 3, n = 6
0h
1h
3h
6h
24h
ISO
ISO
ISO
ISO
ISO
10 min
15 %
C Calcium response
15 %
0h
1h
3h
6h
24h
Neurons
D Calcium astrocyte
N = 3, n = 6
0h
1h
3h
6h
24h
ISO
ISO
ISO
ISO
ISO
10 min
50 %
E Calcium response
50 %
0h
1h
3h
6h
24h
Astrocytes
F Lactate neuron
N = 2, n = 6
0h
1h
3h
6h
24h
ISO
ISO
ISO
ISO
ISO
10 min
2 %
G Lactate surge
2 %×min
0h
1h
3h
6h
24h
Neurons
H Lactate astrocyte
N = 3, n = 6
0h
1h
3h
6h
24h
ISO
ISO
ISO
ISO
ISO
10 min
2 %
I Lactate surge
5 %×min
0h
1h
3h
6h
24h
Astrocytes